HIGH CYCLE FATIGUE
CRACK MODELING AND ANALYSIS
FOR DECK TRUSS FLOORING
CONNECTION DETAILS

Final Report

State Planning and Research
Project Number 5280

by

Anthony H. DePiero
Graduate Research Assistant

Robert K. Paasch, Ph. D.
Professor of Mechanical Engineering

Prepared for

Technical Report Documentation Page

1. Report No. 5280	2. Government Accession No.	3. Recipient's Catalog No.
4. Title and Subtitle High Cycle Fatigue Crack Modeling and Analysis for Deck Truss Flooring Connection Details Phase 10 - Final Documentation		5. Report Date July 1997
		6. Performing Organization Code
7. Author(s) Anthony H. DePiero, Robert K. Paasch		8. Performing Organization Report No.
9. Performing Organization Name and Address Department of Mechanical Engineering 204 Rogers Hall, Oregon State University Corvalli, OR 97331-6001		10. Work Unit No. (Trais)
		11. Contract or Grant No. 13724
12. Sponsoring Agency Name and Address ODOT and FHWA Engineering Services Section Oregon Division Research Unit The Equitable Center 2950 State Street 530 Center St. Salem, OR 97301 Salem OR 97301	10. Type of Report and Period Covered Final Report 1995-1997
		14. Sponsoring Agency Code
15. Supplementary Notes		

16. Abstract

The Oregon Department of Transportation is responsible for many steel deck truss bridges containing connection details that are fatigue prone. A typical bridge, the Winchester Bridge in Roseburg, Oregon, was analyzed to assess the loading conditions, stress levels, and fatigue life of the connection details. The analysis included linear-elastic beam analysis, 2D and 3D finite element modeling, and fatigue modeling. A field identification methodology was developed to expand the analysis to other steel deck truss bridges. Five retrofit strategies were investigated to determine their effectiveness in reducing the stress ranges developed in the connection details.

17. Key Words Steel Deck Truss Bridge, Connection Details, Clip Angles, Fatigue Cracks, Finite Element Analysis, Identification Methodology	18. Distribution Statement Available through the Oregon Department of Transportation Research Unit

19. Security Classif. (of this report) Unclassified	20. Security Classif. (of this page) Unclassified	21. No of pages 56	22. Price

Form DOT F 1700.7 (8-72)   Reproduction of completed page authorized

SI* (MODERN METRIC) CONVERSION FACTORS

APPROXIMATE CONVERSIONS TO SI UNITS

Symbol	When You Know	Multiply By	To Find	Symbol
LENGTH				
in	inches	25.4	millimeters	mm
ft	feet	0.305	meters	m
yd	yards	0.914	meters	m
mi	miles	1.61	kilometers	km
AREA				
in²	square inches	645.2	millimeters squared	mm²
ft²	square feet	0.093	meters squared	m²
yd²	square yards	0.836	meters squared	m²
ac	acres	0.405	hectares	ha
mi²	square miles	2.59	kilometers squared	km²
VOLUME				
fl oz	fluid ounces	29.57	milliliters	mL
gal	gallons	3.785	liters	L
ft³	cubic feet	0.028	meters cubed	m³
yd³	cubic yards	0.765	meters cubed	m³

NOTE: Volumes greater than 1000 L shall be shown in m³.

Symbol	When You Know	Multiply By	To Find	Symbol
MASS				
oz	ounces	28.35	grams	g
lb	pounds	0.454	kilograms	kg
T	short tons (2000 lb)	0.907	megagrams	Mg
TEMPERATURE (exact)				
°F	Fahrenheit temperature	$5(F-32)/9$	Celsius temperature	°C

APPROXIMATE CONVERSIONS FROM SI UNITS

Symbol	When You Know	Multiply By	To Find	Symbol
LENGTH				
mm	millimeters	0.039	inches	in
m	meters	3.28	feet	ft
m	meters	1.09	yards	yd
km	kilometers	0.621	miles	mi
AREA				
mm²	millimeters squared	0.0016	square inches	in²
m²	meters squared	10.764	square feet	ft²
ha	hectares	2.47	acres	ac
km²	kilometers squared	0.386	square miles	mi²
VOLUME				
mL	milliliters	0.034	fluid ounces	fl oz
L	liters	0.264	gallons	gal
m³	meters cubed	35.315	cubic feet	ft³
m³	meters cubed	1.308	cubic yards	yd³
MASS				
g	grams	0.035	ounces	oz
kg	kilograms	2.205	pounds	lb
Mg	megagrams	1.102	short tons (2000 lb)	T
TEMPERATURE (exact)				
°C	Celsius temperature	$1.8 + 32$	Fahrenheit	°F

* SI is the symbol for the International System of Measurement

(4-7-94 jbp)

DISCLAIMER

This document is disseminated under the sponsorship of the Oregon Department of Transportation and the United States Department of Transportation in the interest of information exchange. The State of Oregon and the United States Government assume no liability of its contents or use thereof.

The contents of this report reflect the views of the authors, who are responsible for the facts and the accuracy of the data presented herein. The contents do not necessarily reflect the official policies of the Oregon Department of Transportation or the United States Department of Transportation.

The State of Oregon and the United States Government do not endorse products of manufacturers. Trademarks or manufacturer's names appear herein only because they are considered essential to the object of this document.

This report does not constitute a standard, specification, or regulation.

HIGH CYCLE FATIGUE CRACK MODELING AND ANALYSIS FOR DECK TRUSS FLOORING CONNECTION DETAILS
Final Report

TABLE OF CONTENTS

APPENDICES

LIST OF TABLES

LIST OF FIGURES

1.0 INTRODUCTION

The Oregon Department of Transportation (ODOT) is responsible for approximately 320 steel bridges, many of which have flooring system connection details that are fatigue prone. Over 20 structures have been found to have details with fatigue cracks. The majority of these bridges built prior to 1960, have details nearing the end of their fatigue life and will require increased inspection and repair over the next 10 to 20 years. Bridges on major routes require added attention since they can experience as many as 1 to 5 million significant load cycles per year. Some of these bridges have over 1000 connection details making the cost of inspection and repair very expensive.

The need to quantify the fatigue condition of these connection details is apparent. It is driven by the desire to limit inspection and to repair or replace only details with potential problems. The need exists to accurately assess the loading conditions and fatigue crack growth rate for the connection details and to develop a low cost field identification methodology to identify problem details. The current procedure is to repair only those connection details that currently contain visible fatigue cracks. Other connection details are left in service even though they may be nearing the end of their serviceable life. A more economic repair procedure could be implemented if there is detailed knowledge about which details are nearing the end of their fatigue life.

The goal of this research is to accurately assess the loading conditions and the fatigue crack growth rate for the connection details of a specific bridge, the Winchester Bridge on Interstate 5 in Roseburg, Oregon. Even though the analysis is being performed for this specific bridge, there is an expectation that the procedure, and to some degree, the results, can be applied to other bridges. Figure 1.1 shows a flowchart of the different phases of the project.
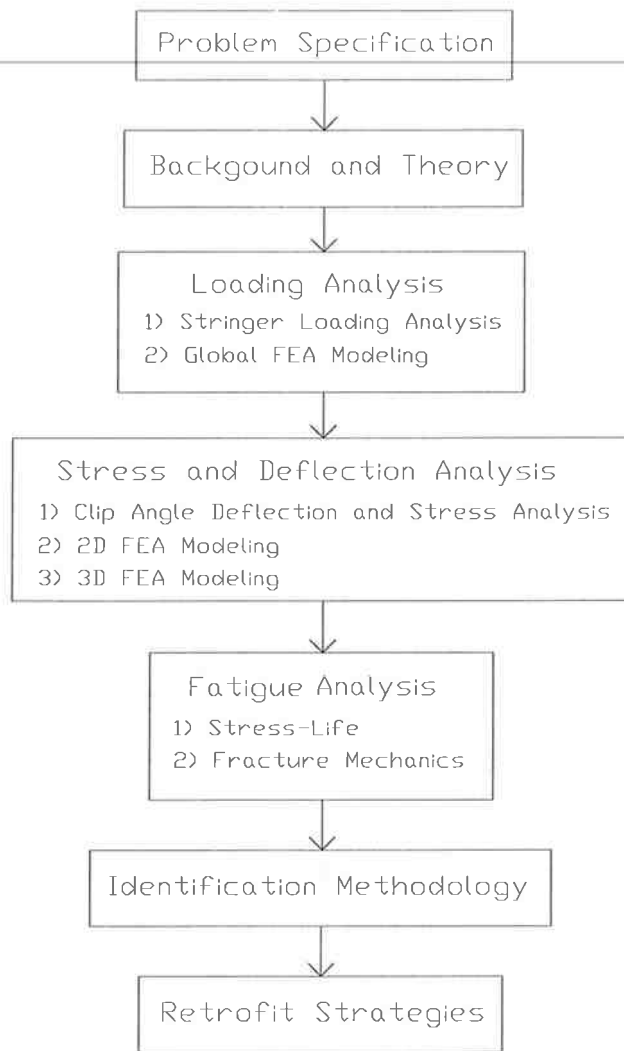
Figure 1.1 Flow chart of the project phases.

Problem specifications are discussed in Chapter 2; the specific bridge for study is identified and described. The Loading Analysis is addressed in Chapter 4 and includes a discussion of the two analysis methods used to determine the loading on the stringers (beams attached to connection details). In Chapter 5, Stress and Deflection Analysis, the deflections and stress ranges of the connection details are quantified. Detailed finite element models are used extensively in the both the Loading Analysis and the Deflection and Stress Analysis. Hand calculations are used to gain insight into and guide the development of the finite element models. Experimental data are used to validate the analysis. Chapter 6 covers the Fatigue Analysis and includes reviews of the two methods used for estimating the connection details' remaining life. The development of a low cost field identification methodology to identify problem connection details is discussed in Chapter 7. In Chapter 8 results are presented from the investigation of five retrofit strategies. The project is summarized in Chapter 9.

2.0 PROBLEM SPECIFICATION

The Winchester Bridge is a typical steel deck truss bridge under the responsibility of ODOT that has experienced high cycle fatigue problems in its flooring system connection details. For this reason, the Winchester Bridge was selected for study.

The Winchester Bridge, located on Interstate 5, five miles north of Roseburg, Oregon, spans the North Fork of the Umpqua River. The bridge has separate north and southbound structures that were constructed in 1953 and 1963, respectively. The two structures are very similar in their construction. Each structure is made of six, 140 foot steel deck truss spans. Figure 2.1 illustrates one span of the southbound structure without the reinforced concrete deck. The spans are separated by expansion joints
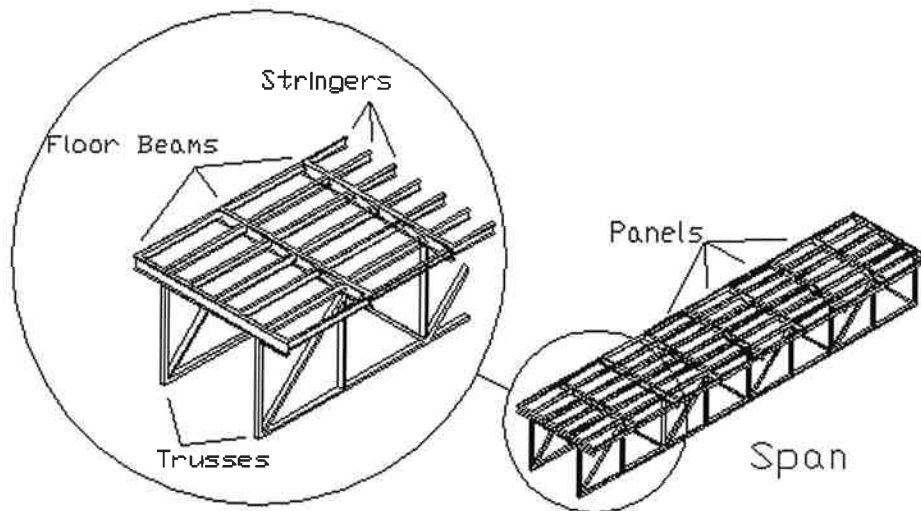
Figure 2.1 Diagram of one span of the southbound structure of the Winchester Bridge without the six inch concrete deck.

making them independent of one another. Each span is made up of a pair of steel trusses whose center lines are 20 feet apart. Each pair of trusses supports nine laterally oriented floor beams that are 17.5 feet apart. The sections between the floor beams are called "panels". The northbound structure has five stringers in each panel running between the floor beams. The southbound structure has seven stringers in each panel. A six inch thick reinforced concrete deck lays on top of the floor beams and stringers. The north and southbound structures have slightly different size floor beams and stringers. In the northbound structure the floor beams are W24 x

76 wide flange steel beams and the stringers are W18 x 50 wide flange steel beams. In the southbound structure the floor beams are W27 x 84 wide flange steel beams and the stringers are W18 x 45 wide flange steel beams.

It is in the connection details (or clip angles) that connect the stringers to the floor beams that fatigue cracks have been found. Figure 2.2 shows a typical connection detail assembly.
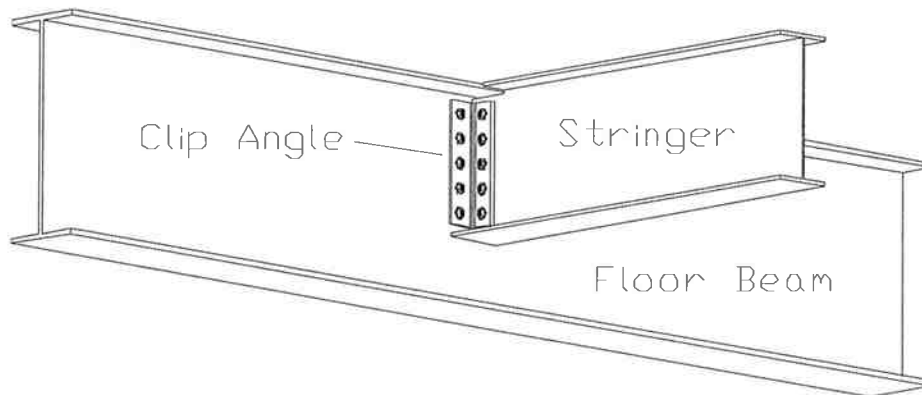
Figure 2.2 Typical stringer to floor beam connection detail assembly.

Figure 2.3 illustrates the clip angle used in the stringer to floor beam connection assemblies on the Winchester Bridge. The clip angles are connected to the stringers and floor beams using $\frac{7}{8}$
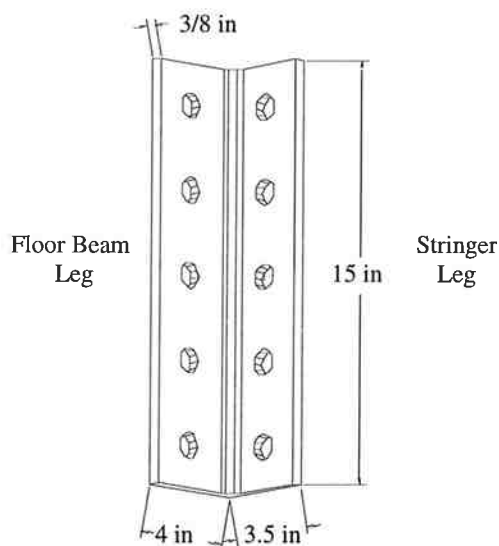
Figure 2.3 Clip angle used in the stringer to floor beam assemblies on the Winchester Bridge.

inch diameter rivets. Rivet holes are positioned 1.5 inches from the edges and spaced 3 inches apart on center.

The primary function of the clip angles is to transmit the shear from the stringer to the floor beam. Because they are riveted to both the stringer and floor beam, the angles are subjected to flexural stresses caused by the vertical deflection of the stringer under wheel loads. As the stringer deflects, the rotation of the end of the stringer subjects the connection detail to a flexural moment.

Fatigue cracks as long as four inches have been found in the clip angles. The cracks have been located at the corner of the clip angle running vertically from the top of the clip angle down. The fracture surface of the cracks have been oriented at an angle of approximately 45 degrees to the legs of the clip angle. Figure 2.4 illustrates a clip angle with a typical fatigue crack.
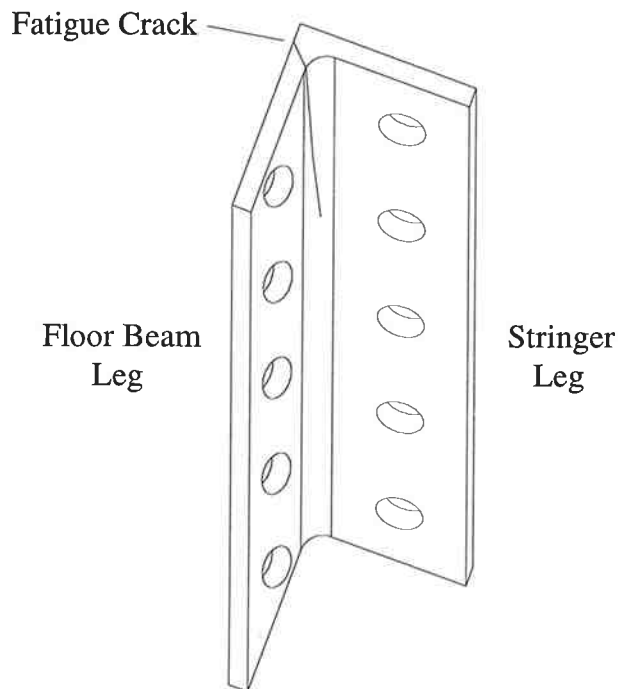
Figure 2.4 Clip angle with a typical fatigue crack.

In 1994, repair was conducted on both the north and southbound structures of the Winchester Bridge. Thirteen cracked clip angles were replaced on the southbound structure at a cost of $16,384. Similar work was performed on the northbound structure at a cost of $16,296.

The north and southbound structures of the Winchester Bridge are logical choices on which to perform a detailed analysis. The structures are typical steel deck truss bridges which have both had significant fatigue problems and experience a high number of load cycles per year. They are also crucial structures for the transportation of people and goods through the interstate corridor.

3.0 BACKGROUND AND THEORY

The first step in solving a problem is to first establish what research has already been performed that can assist in solving that problem. The examination of research performed on similar projects can give insight and help in understanding the problem currently being studied.

The connection angles in a study of railway bridge connection angles performed by Wilson of the University of Illinois [Wilson, 1940] are very similar to the clip angles used on the Winchester Bridge. A finite element analysis and field testing were performed by [Cao et al, 1996] on a Colorado State Route 224 bridge over the South Platte River near Commerce City. The National Cooperative Highway Research Program (NCHRP) Report 299, *Fatigue Evaluation Procedures for Steel Bridges* [Moses, et al, 1987] contains comprehensive fatigue evaluation procedures developed to guide the fatigue evaluation of existing bridges. The NCHRP Report 299, the study of the reinforced concrete deck, and Wilson's study on railway bridge connection details are discussed in the following section.

Basic principles and theory are used as tools in research. For this project the use and understanding of finite element analysis (FEA) and fatigue theory are very important. FEA and the FEA modeling tools used in this research, as well as three methods of fatigue analysis are reviewed in the following sections.

3.1 BACKGROUND

Fatigue in bridges has been a concern to the transportation community for many years. Studies of connection angles for stringers of railway bridges were performed in the late 1930's by Wilson and Coombe of the University of Illinois [Wilson, 1940] and [Wilson and Coombe, 1939]. Both computational analysis and fatigue testing were performed. The connection details that Wilson studied experience flexural stresses due to deformation of the bridge. There are two actions that contributed to these flexural stresses.

The first was the lengthening of the bottom chord of the truss with passage of a train. The stringers did not experience a corresponding change in length and since the floor beams are connected to both bottom chord and the stringers an axial force was produced and transmitted through the connection angles. One stress cycle was completed for each passage of a train.

The second action was the vertical deflection of the stringer under each set of wheels. The deflection rotated the end of the stringer and subjected the connection detail to a flexural moment. Stress cycles from this action were repeated for the passage of each car.

Wilson concluded that, because the stress in a flexural member varies as the square of the length, the stress state is much worse for connection details with short stiff legs than those with longer more flexible legs [Wilson, 1940].

Nine connection details of three different configurations were fatigue tested by repeatedly applying axial loads. The tests were designed to find the fatigue strengths of both connection angles and rivets [Wilson and Coombe, 1939].

The purpose of the study on the reinforced concrete bridge decks was to determine whether the top transverse reinforcing bars in the deck are necessary to sustain the negative bending moments and the tensile stresses seen in the top of the deck over the girders. The motivation for eliminating the top transverse reinforcing bars is that they are most susceptible to corrosion from deicing chemicals. [Cao, et al, 1996]

A finite element model was used in conjunction with experimental testing to determine the stress of the deck over the girders. Both the concrete deck and the girders were modeled. The concrete deck in the vicinity of the load points was modeled using a two layers of solid elements. The girders were modeled using 3D beam elements. Rigid beam elements were used to connect the nodes on the bottom of the deck to the centroid of the girders. In areas away from the load points equivalent beam elements were used to model the combination of the deck and the girders. [Cao, et al, 1996]

A substantial amount of research has been done to develop fatigue evaluation procedures for bridges. The National Cooperative Highway Research Program (NCHRP) Report 299, *Fatigue Evaluation Procedures for Steel Bridges* [Moses, et al, 1987] is a comprehensive report that outlines procedures for evaluating the fatigue condition of existing steel bridges. Loading issues, such as the proposed standard fatigue truck, impact, truck superposition, and cycles per truck passage, are discussed. The report contains methods for calculating moment ranges, stress ranges and the remaining fatigue life. Options for different levels of effort that reduce uncertainties and improve predictions of remaining life are presented. The evaluation procedures provided an effective guide to developing the analysis methods used in the project.

3.2 FINITE ELEMENT ANALYSIS

The finite element method, which was introduced in the late 1950's, is a type of computer simulation that is used to perform computational mechanics. The component of interest is first divided up into many small boxes or elements. The elements can have irregular shapes and conform closely to the shape of the component being modeled. The collection of elements forms a three-dimensional grid or mesh and makes the object look as though it is made of small building blocks. Nodes are points in the mesh where elements are connected. Discrete equations are used to mathematically couple adjacent nodes of the mesh to one another. Although the equations couple only adjacent nodes, they are derived from global balance laws. The following sections discuss the finite element method modeling tools that are used in the global FEA model, the 2D FEA model, and the 3D FEA model.

3.2.1 GLOBAL FEA MODELING

COSMOS/M was used to perform the finite element macro modeling. COSMOS/M is a modular, self-contained finite element system developed by Structural Research and Analysis Corporation [*COSMOS/M User's Guide*, 1992]. The module GEOSTAR was used as the mesh generator and post-processor. The STAR module was used for the linear static analysis of the deck structure. Other modules are available with a variety of different modeling capabilities.

3.2.2 2D FEA MODELING

The 2D modeling was performed using codes developed by the Methods Development Group at Lawrence Livermore National Laboratory (LLNL). MAZE was used to generate the mesh. It was developed as a mesh generator for the LLNL family of 2D FEA codes. [Hallquist, 1983]

NIKE2D was used to perform the analysis. This program is a nonlinear, implicit, 2D finite element code for solid mechanics. It uses a variety of elastic and inelastic material models. It has slide line algorithms that permit gaps, frictional sliding, and single surface contact along material interfaces. [Engelmann, 1991]

ORION was used to view the results generated by NIKE2D. It is an interactive color post-processor developed to view the results of the 2D FEA codes at LLNL. [Hallquist and Levatin, 1992]

3.2.3 3D FEA MODELING

Mesh generation for the 3D FEA model was performed using INGRID and later using TrueGrid. INGRID is a generalized 3D finite element mesh generator developed by the Methods Development Group at LLNL. It has the capability of generating complex geometrical models of nonlinear systems with beam, shell, and hexahedral elements. [Christon and Dovey, 1992]

TrueGrid is a highly interactive mesh generator for wide range of 3D FEA codes. It is similar to INGRID and will generate complex meshes using beam, shell, and hexahedral elements. It was developed by XYZ Scientific Applications, Inc. [*TrueGrid User's Manual*, 1995]

The FEA codes used for the 3D modeling were NIKE3D and LS-NIKE3D. NIKE3D is a nonlinear, implicit, 3D finite element code for solid and structural mechanics. NIKE3D uses beam, shell, and hexahedral elements and a variety of elastic and inelastic material models. It has contact-impact algorithms that permit gaps, frictional sliding, and mesh discontinuities along material interfaces. NIKE3D was originally developed by John Hallquist of the Methods Development Group at LLNL, with continued development by Bradley Maker and Robert Ferencz. [Maker, 1991]

LS-NIKE3D is an implicit, finite-deformation, finite element code for analyzing the static and dynamic response of three dimensional solids. LS-NIKE3D was developed by Livermore Software Technology Corporation (LSTC) from the NIKE3D code developed at LLNL. Major developments made in the contact algorithms and the linear equation solving technology have made LS-NIKE3D robust and efficient. [*LS-NIKE3D User's Manual*, 1996]

The post processor used to view the results generated by the 3D FEA code was LS-TAURUS. LS-TAURUS is a highly interactive post-processor developed by LSTC to display results of LLNL and LSTC families of 3D FEA codes. It originated from LLNL post-processors developed by John O. Hallquist. [*LS-TAURUS User's Manual*, 1995]

3.3 FATIGUE

Fatigue is the process responsible for premature failure or damage of components subjected to repeated loading [Bannantine and Comer, 1990]. Fatigue is considered low cycle if the number of load cycles to failure is less than 1000 cycles, and high cycle if the number of load cycles to failure is more than 1000 cycles. Fatigue is often divided into two phases; crack initiation and crack propagation. Crack initiation is the phase where a crack is formed, usually around an inclusion or other defect. Crack propagation occurs when the crack increases in length with subsequent load cycles. The boundary between the two phases is often very difficult to determine.

Three general methods of fatigue analysis are used in analysis and design. They are strain-life, stress-life, and linear-elastic fracture mechanics. Each method has both strengths and weaknesses and each may be more appropriate for different classes of problems. Knowledge about the material, loading, geometry, whether the fatigue is low or high cycle, and whether the phase of interest is initiation and/or propagation is helpful in determining which method is most appropriate.

3.3.1 STRAIN-LIFE FATIGUE ANALYSIS

The strain-life method uses the true strain to predict the number of cycles to failure. When components are under high load and/or have critical locations (notches), the stress-strain relationship is no longer linearly related. In these situations. the plastic strain becomes a significant part of the deformation. Since the primary mechanism in fatigue is plastic deformation, an elastic model is not appropriate. The strain-life method uses the level of deformation explicitly, and it is more appropriate for cases with high plastic deformation. These types of cases fall into the low cycle fatigue category.

The strain-life method is used by comparing the true strain range to a strain vs. fatigue life curve. One weakness of this method is that finding true strain in areas of discontinuities can be very difficult. More experimental data is needed to account for surface finish, surface treatment, loading, and other modifying parameters.

3.3.2 STRESS-LIFE FATIGUE ANALYSIS

The stress-life method uses the alternating stress amplitude to predict the number of cycles to failure. This method is based on comparing the stress amplitude to a stress vs. fatigue life curve, S-N diagram. These curves are based on empirical formulas derived from experimental data. The stress-life method is generally only used for high cycle fatigue because under low cycle fatigue, the stress-strain relationship becomes nonlinear.

For many metals (including steel) there exists a region of infinite life, where fatigue problems will not develop if the stress amplitude is below a threshold value. This threshold value is called the endurance limit (S_e) [Shigley and Mischke, 1989]. In many materials, the endurance limit has been related to the ultimate tensile strength (S_{UT}) through experimental testing. The ideal endurance limit (S_e') for steels with a ultimate tensile strength less than 200 ksi is roughly $0.5 \cdot S_{UT}$ [Shigley and Mischke, 1989]. The ideal endurance limit is calculated in a laboratory where the conditions of the experiment and the specimen are carefully controlled. The ideal endurance limit is then related to the actual endurance limit by applying factors that account for differences in surface finish, surface treatments, size, temperature, loading, and other environment factors [Bannantine and Comer, 1990].

The S-N diagram is a log scale plot of the fully reversed stress amplitude vs. the number of stress cycles to failure. For steel, the S-N diagram is generally drawn by connecting a line from the fatigue strength at 10^3 cycles to the endurance limit (S_e) at 10^6 cycles. The fatigue strength at 10^3 is only slightly less than the S_{UT} and is taken to be $0.9 \cdot S_{UT}$. [Shigley and Mischke, 1989]

For the cases where the stress mean is not zero, an equivalent stress amplitude (S) must be calculated from the mean stress (σ_m) and the stress amplitude (σ_a). There are two relationships that tend to bracket the test data. They are the Goodman and Gerber relationships. The equations are shown below. The Goodman relationship is the more conservative of the two and is often used for that reason. [Bannantine and Comer, 1990]

Goodman Relationship
$$S = \frac{\sigma_a}{1 - \dfrac{\sigma_m}{S_{UT}}}$$
(3-1)

Gerber Relationship
$$S = \frac{\sigma_a}{1 - \left(\dfrac{\sigma_m}{S_{UT}}\right)^2}$$
(3-2)

The endurance limit is based on a constant amplitude alternating stress. There are many instances where the stress amplitude is variable. In these cases, a method for calculating cumulative damage is used to find an effective alternating stress. A root mean cubed method is often used to estimate cumulative damage [Moses, et al, 1987]. The individual stress range values are first cubed, an average is taken, and then the cube root of the average is determined. The result is a effective stress range value that is larger than the value obtained from the arithmetic average because cubing the stress range values increases the emphasis on the large values in the distribution. If the alternating stress is not fully reversed, an equivalent stress amplitude is then calculated using either the Goodman or Gerber relationship.

Even though the effective stress amplitude may be less than the fatigue limit, many amplitudes may still fall above the fatigue limit. This typically results in a finite life. Distributions with as low as one stress amplitude in thousand above the fatigue limit have still been found to exhibit a finite life [Fisher, et al, 1983].

One method of calculating the finite life for variable amplitude alternating stress is to extend the S-N curve beyond the constant amplitude fatigue limit [Moses, et al, 1987]. The slope of this extension can be adjusted to reflect the distribution of cycles above the constant amplitude fatigue limit.

The stress-life method is completely empirical in nature and is limited to cases of high cycle fatigue only. It has, however, been used for many years and there is a considerable amount of experimental data that has been used to derive empirical solutions.

3.3.3 LINEAR-ELASTIC FRACTURE MECHANICS

Linear-elastic fracture mechanics (LEFM) is an analytical method that relates the stress at a crack tip to the nominal stress field around the crack. LEFM began with Griffith's work in the 1920's. Griffith proposed that for brittle materials a crack will propagate if the total energy of the system is reduced by the propagation. In the 1940's, progress continued with Irwin's work; a theory for ductile materials was added. Irwin reported that the energy applied to plastic deformation must be included by adding it to the surface energy associated with the new crack surface. In the 1950's, Irwin also developed equations for the local stresses near the crack tip. [Bannantine and Comer, 1990]

There are three modes describing crack displacement: Mode I; opening or tensile mode, Mode II; sliding or in-plane shear, and Mode III; tearing or anti-plane shear. Figure 3.1 shows a schematic representation of each of these three modes. For most structures Mode I is the dominate condition.
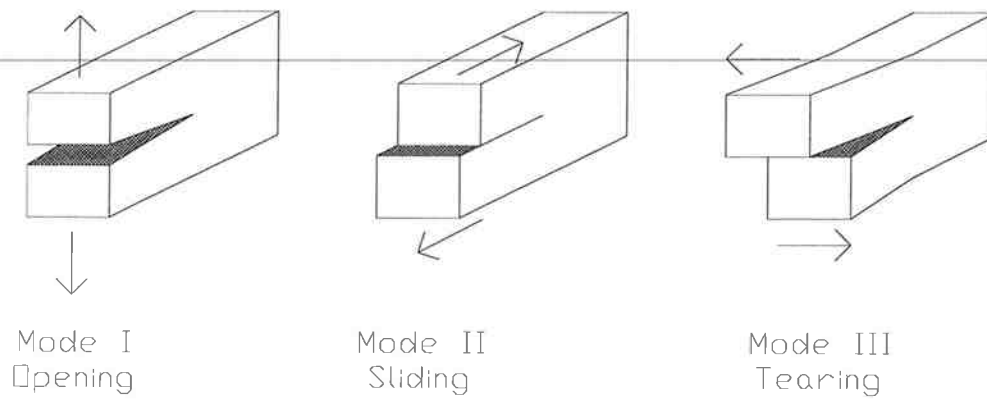
Figure 3.1 Three modes of crack displacement.

With the existence of a crack, there is an infinite stress concentration at the crack tip. The stress intensity factor, K, allows the singularity to be dealt with in terms of strain energy. The stress intensity factor describes the entire stress state around the crack tip. K is a function of the nominal stress, crack length, and geometric factors. The stress intensity factor is described by [Fisher, et al, 1989] as

$$K = F_e \cdot F_s \cdot F_w \cdot F_g \cdot \sigma \cdot \sqrt{\pi \cdot a} \qquad\qquad (3\text{-}3)$$

where a is the crack length for an edge crack and half the crack length for an internal crack, σ is the nominal tensile stress normal to the crack plane, F_e is a factor for crack shape, F_s is a factor to account for surface cracks, F_w is a factor for a specimen with finite width, and F_g is a factor for non-uniform nominal stress.

If the stress intensity at the crack tip reaches a critical value the crack will begin unstable propagation. This critical stress intensity is called the fracture toughness (K_C). The fracture toughness can be used to calculate the critical crack length at which unstable propagation will occur. For Mode I crack displacement with plane strain conditions existing at the crack tip, the fracture toughness is denoted by K_{IC}. K_{IC} values are obtained by using the standard ASTM test method, E-399-83 [Barsom and Rolfe, 1987].

There are three regions of the fatigue crack growth. Region I includes the initiation stage where the crack growth rate is small and threshold effects are important. Region II is a region of consistent and predictable crack growth rate. Region III is a region of rapid and unstable crack growth rate. Generally, region III does not contribute significantly to the fatigue life and is ignored [Bannantine and Comer, 1990].

The stress intensity can be related to the fatigue crack growth rate, (da/dN). When the stress field around a crack is alternating this produces an analogous alternating stress intensity factor (ΔK). ΔK is calculated the same as K except that σ is replaced by $\Delta\sigma$. In Region II the slope of the log da/dN versus the log ΔK curve is linear, and da/dN and ΔK are related by the Paris equation from [Shigley and Mischke, 1989]

$$\frac{da}{dN} = C \cdot [\Delta K(a)]^M \qquad (3\text{-}4)$$

where da/dN is the crack growth rate, ΔK is the alternating stress intensity factor, N is the number of cycles, and C and M are empirical constants of the material. The fatigue life is determined by evaluating the integral

$$N = \int_{a_i}^{a_f} \frac{1}{C \cdot [\Delta K(a)]^M} \, da \qquad (3\text{-}5)$$

where a_i is the initial crack size, a_f is the final crack size. The final crack size is usually set as the critical crack size. The initial crack size is often set as the size of largest defect that is expected to be present. The largest defect size is often difficult to determine. The initial crack size is very important because, when the crack length is small, the crack growth rate is also very small.

4.0 LOADING ANALYSIS

This chapter describes two analysis methods used to calculate the distribution of live truck loads on the stringers. The first method, stringer loading analysis is a linear-elastic analysis hand calculation. The second method, the global FEA model, was performed using the finite element method. A model validation analysis of the global FEA model is also discussed. The live loading results of the two analyses are also presented in section 4.3.

For both analysis methods, the suggested standard fatigue truck, outlined in the NCHRP Report 299 [Moses, et al, 1987], is used for model loading. Figure 4.1 shows a diagram of the standard fatigue truck. This truck was developed to represent the variety of different types and weights of
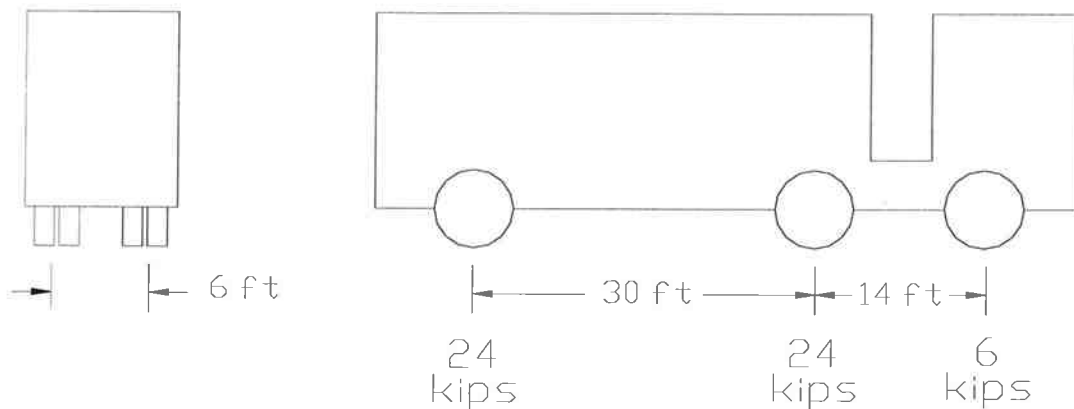
Figure 4.1 Suggested standard fatigue truck outlined in the NCHRP Report 299.

trucks in actual traffic. It consists of two rear axles of 24 kip each and a front axle of 6 kip. The rear axles are spaced 30 feet while the front and the first rear axle are spaced 14 feet. The width of each axle is 6 feet.

4.1 STRINGER LOADING ANALYSIS

The distribution of the truck loads through the deck on the stringers is important in determining the loading on the clip angle. The loads on each stringer were calculated with one rear axle of the fatigue truck positioned longitudinally in the center of a panel over the mid length of the stringers. Laterally, the axle was centered in the slow lane of traffic. For both the north and southbound structures, three stringers are assumed to carry the entire weight of the axle. Those

stringers are the middle stringer, the 2nd from the middle stringer, and the 3rd from the middle stringer in the slow lane. Figure 4.2 shows a diagram of the location of the three stringers.
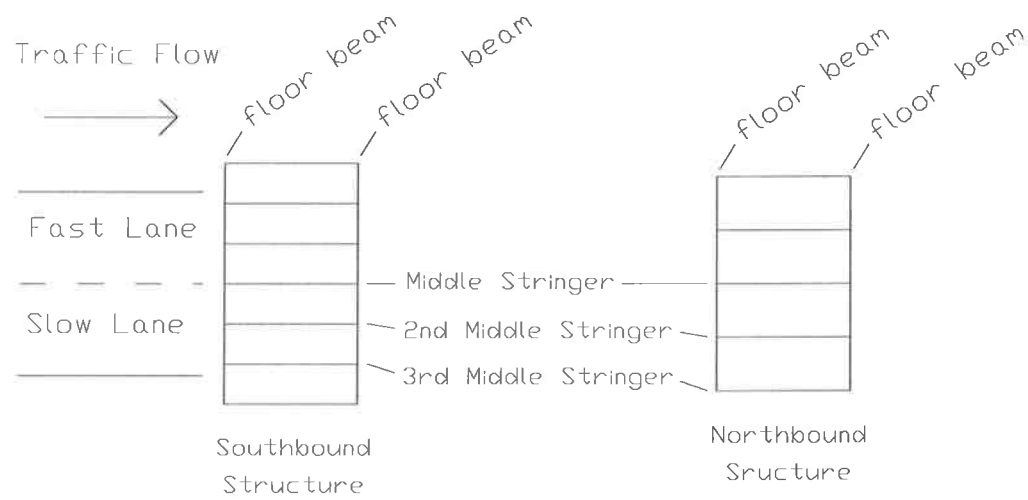
Figure 4.2 Top view diagram of the three stringers that are assumed to carry the axle load in the stringer loading analysis.

Each section of the deck between the three stringers was analyzed as an independent beam using beam tables from [Shigley and Mischke, 1989]. The stringer loads were calculated as the reaction forces at the ends of the beams. Figure 4.3 shows a diagram of the loading and boundary conditions. The stringer loads for both the north and southbound structures can be found in results section. For details of the analysis see Appendix A.
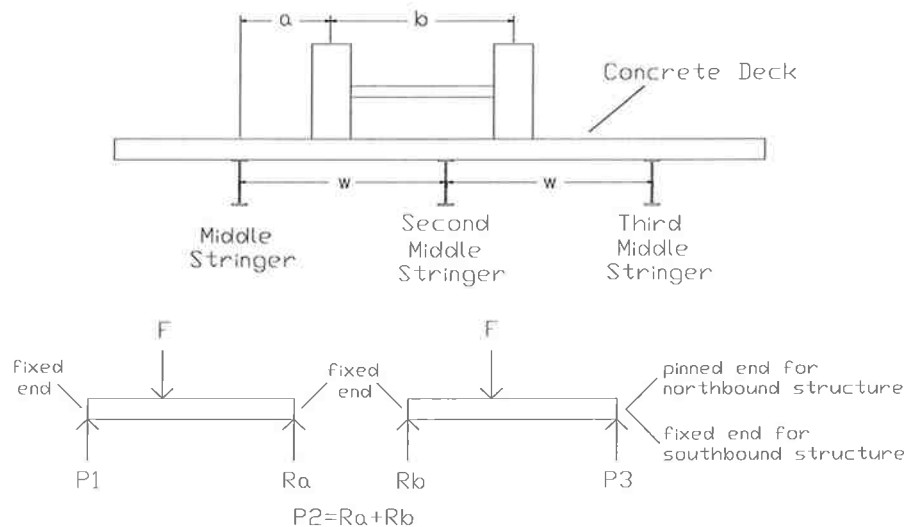
Figure 4.3 Diagram of the loading and boundary conditions used in the stringer loading analysis.

16

4.2 GLOBAL FEA MODEL

Finite element models for both the north and southbound structures were developed to determine the distribution of loads on the stringers. The floor beams, stringers, clip angles, and the reinforced concrete deck of one panel are included in the model. 3D beam elements were used to model the floor beams and stringers. Orthotropic plate elements were used to model the reinforced concrete deck. The properties of the orthotropic plate elements were determined by performing an analysis of the reinforced concrete deck. Discussion of this analysis can be found in the following section.

Beam elements with a length of 0.1 inches were used to model the boundary conditions created by the clip angles and floor beams. Because the boundary beam elements modeled the compliance of the floor beams, the rotation of the floor beams were fixed. The area moment of inertia of the boundary beam elements was set so that the end rotation at the end of the stringer beam elements matched the rotation of the clip angle from the clip angle deflection analysis. When results became available from the 3D FEA model, the properties of the boundary beam elements were adjusted. Two boundary beam elements were developed from the results of the 3D FEA model. One modeled the connection details in the interior of the span, and the other modeled the connection details at the end of the span.

Models of both an end panel and an interior panel were developed for each of the north and southbound structures. One axle of the standard fatigue truck was used to load the models. The distribution of loads on the stringers were the primary interest. It was observed that the properties of the boundary beam elements, the area moment of inertia of the stringers, and the longitudinal position of the axle did not play a significant role in the loading of the stringers. Individual loading on the stringers is strongly dependent upon both the lateral position and the width of the load axle. This indicates that detailed knowledge about the position of the stringers in relationship to the lanes of traffic is important. It also demonstrates the necessity of having a fatigue truck that accurately represents the population of trucks.

The stringer loads calculated from the global FEA model can be found in section 4.3. The COSMOS command files can be found in Appendix B.

4.2.1 REINFORCED CONCRETE DECK ANALYSIS

A six inch thick reinforced concrete deck is used to transmit the traffic load to the stringers and floor beams. An analysis was performed to quantify the equivalent stiffness of the concrete deck. During construction rebar was inserted in both the longitudinal and transverse directions to give the deck the tensile strength it needs to support the traffic loads. The position and amount of rebar added in each direction is different. For this reason, it was necessary to quantify the reinforced concrete deck stiffness properties in each direction separately.

17

The orthotropic properties of the deck were calculated by following the procedure outlined in *Reinforced Concrete Design* [Everard and Tanner, 1966]. The properties in each direction were calculated independently. A beam of unit width, with the top portion of the beam associated with compression and the bottom portion associated with tension, was used to model the deck. The reinforcing steel in the top region of the deck was placed in the compression portion of the deck and the steel in the bottom portion of the deck was placed in the tension portion. One exception was made however. In the transverse direction sections of the rebar change depth. The rebar was installed so that it was always in the portion of the deck that would be in tension. It is in the upper region of the deck over the stringers and is in the lower region between the stringers. For this reason, it was placed in the tension portion of the model.

The assumption that the concrete could only contribute strength in compression was used in the analysis. This created a beam model that had concrete and steel on the compression side and steel alone on the tension side. Area moments of inertia per unit width were calculated for both the transverse and longitudinal directions. These area moments of inertia were then used to find equivalent moduli of elasticity for a six inch thick uniform deck. The resulting moduli of elasticity for the transverse and longitudinal directions were 1300 ksi and 546 ksi, respectively. See Appendix C for details of the analysis.

4.2.2 Model Validation

Field testing was performed on the Winchester Bridge by the Oregon Department of Transportation to quantify the live loading and to assist in validating the analysis. Five strain gages were installed on the top of the bottom flanges at mid span of three stringers and two floor beams of one span of the northbound structure. The uniaxial, 350 ohm strain gages had a gage length of 0.25 inches and were used in a three wire quarter bridge configuration. Samples were taken at a rate of 60 Hz with a 30 Hz low pass filter. The sensitivity of the strain measurements is +/- 10 microstrain.

Strain gauges were installed on the first and second floor beams of the first span. Two stringers from the first panel and one stringer from the second panel were installed with strain gages. Figure 4.4 shows the stringers and floor beams that were gauged.
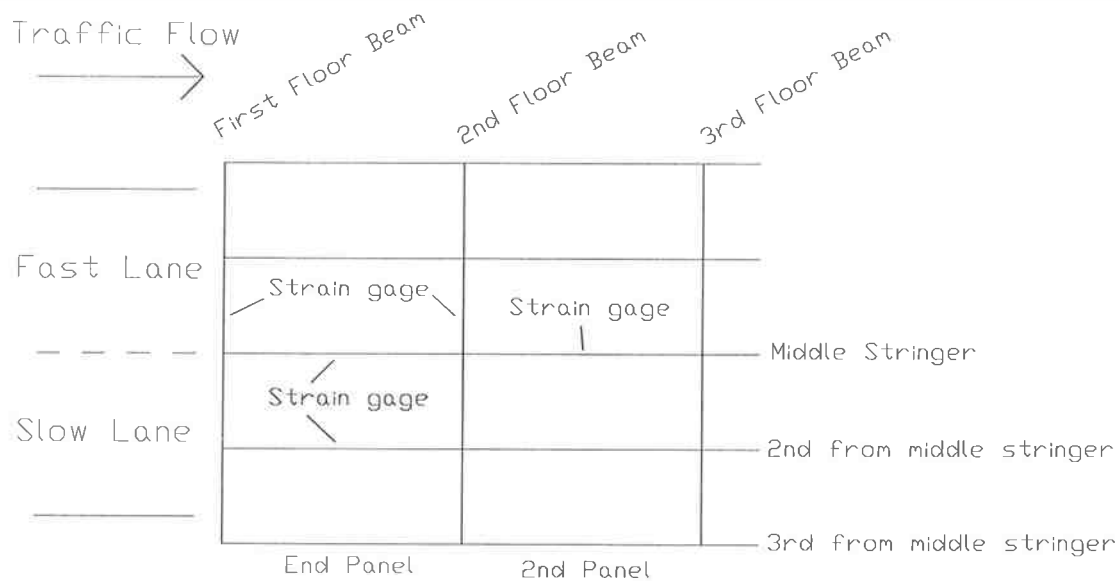
Figure 4.4 Three stringers and two floor beams on the northbound structure of the Winchester Bridge that had strain gauges installed.

In the first panel, the middle stringer and the second from middle stringer in the slow lane had strain gages installed. In the second panel, the second from the middle stringer in the slow lane had a strain gage installed.

Data were taken under normal traffic flow with both lanes open and under a known truck weight with the slow lane closed. Figure 4.5 shows the comparison of the measured stress ranges in the stringer to those calculated from the global FEA model for the known truck weight. Stress ranges from the known truck weight are compared to the stress ranges calculated in the global FEA model loaded with the known truck weight. Figure 4.6 shows the comparison of the measured stress ranges in the stringers to those calculated from the global FEA model for random truck traffic. The cubed-root mean of the measured stress ranges for the random truck traffic are compared to the stress ranges calculated in the global FEA model loaded with the standard fatigue truck.

Figure 4.5 Graph of the stringer stress ranges from the global FEA model and those measured experimentally, loaded with a known truck weight.

Figure 4.6 Graph of the stringer stress ranges from the global FEA model and those measured experimentally, under random traffic loading.

The measured stresses are much lower than those calculated from the global FEA model. This indicates that the composite interaction between the deck and the stringers, an interaction that is not modeled in the global FEA model, is 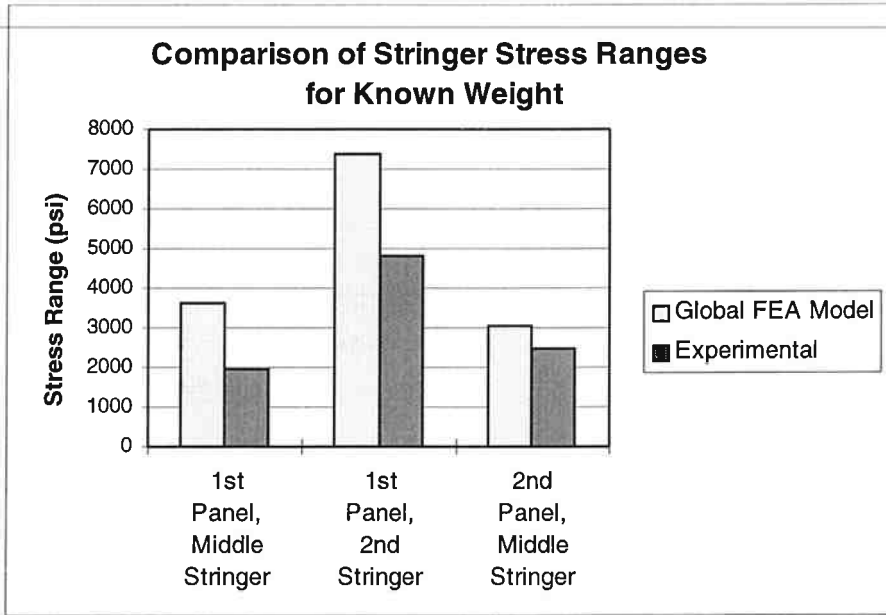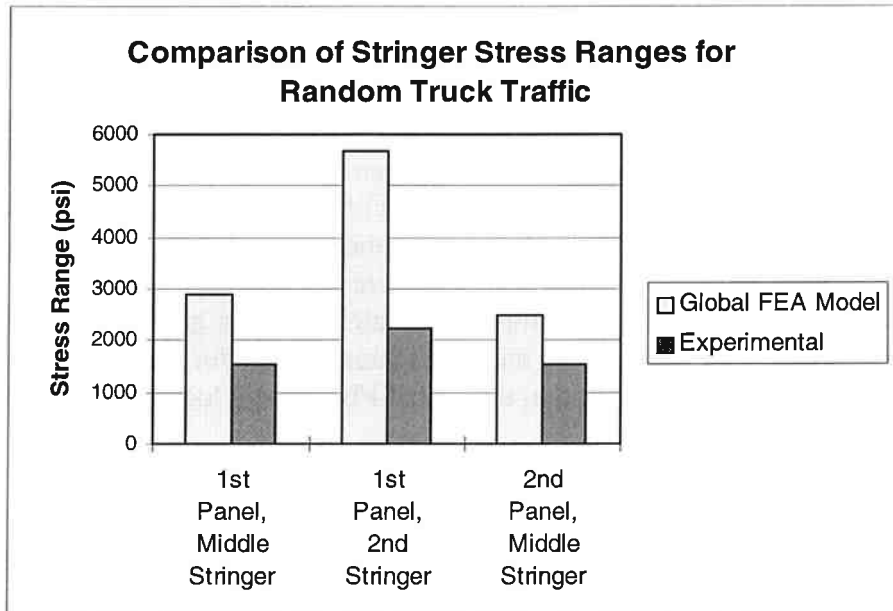important. If shear loads are transferred between the deck and the stringers, the neutral axis is shifted upward and the area moment of inertia is increased. The effect is that the section modulus for the stringer is increased, resulting in a lower stress range.

The composite interaction between the deck and the stringers could be quantified if strain data were available for both the top and bottom flanges. The ratio of strain ranges could be used to calculate the position of the neutral axis, and the known load and the strain range of the bottom flange could be used to calculate the section modulus. The effective area moment of inertia could then be calculated from the new position of the neutral axis and the new section modulus.

Another possible reason, for the difference in calculated and measured stress ranges, is that the actual reinforced concrete deck is stiffer than was calculated. Assuming that concrete only contributes strength in compression is a conservative assumption. A stiffer deck would increase the distribution of the axle load to other stringers.

4.3 RESULTS

Two stringers in each panel of the northbound structure are loaded significantly. A significant load was considered to be one that was greater than 3000 lb. They are the middle stringer and the 2nd from middle stringer on the slow lane side. Three stringers in each panel of the southbound structure are loaded significantly. They are the middle stringer, 2nd from the middle stringer, and the 3rd from middle stringer on the slow lane side. Figure 4.7 is a graph of the stringer loads for the northbound structure. Figure 4.8 is a graph of the stringer loads for the southbound structure.

Stringer Live Loads for Northbound Structure
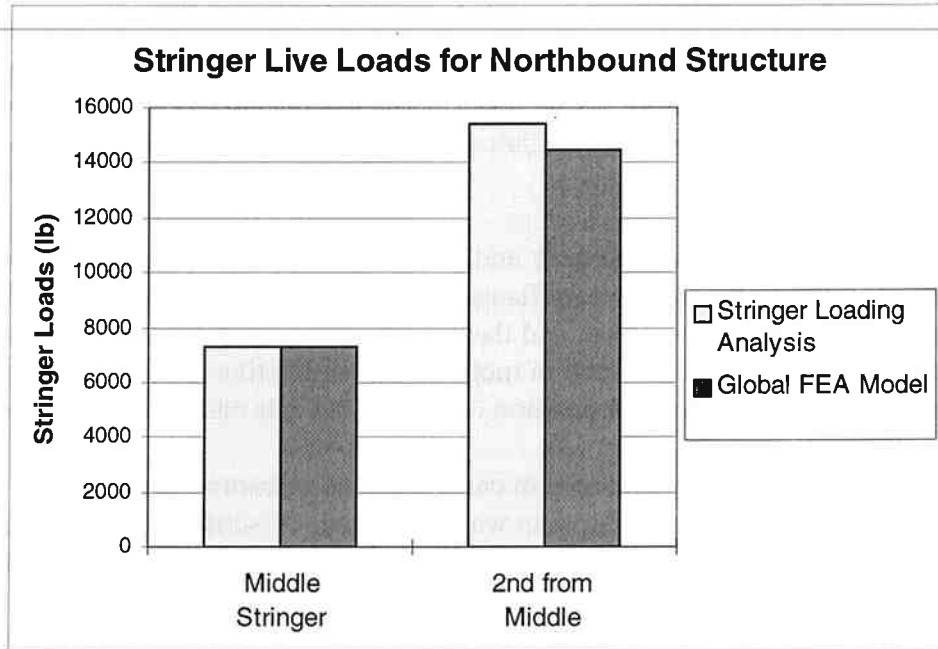
Figure 4.7 Graph of the stringer loads for the northbound structure for both the stringer loading analysis and the global FEA model.

Stringer Live Loads for Southbound Structure
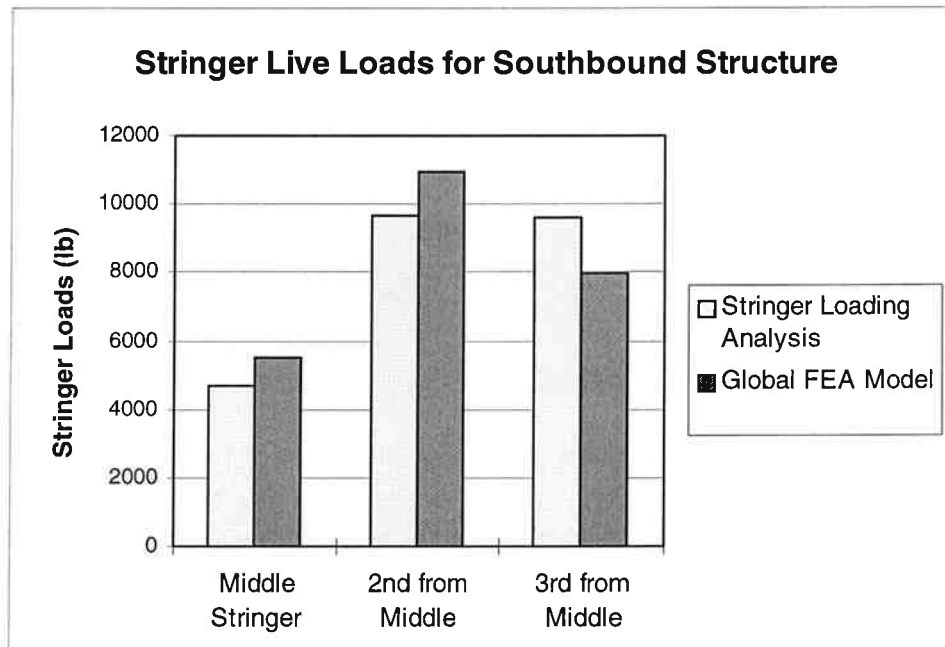
Figure 4.8 Graph of the stringer loads for the southbound structure for both the stringer loading analysis and the global FEA model.

22

It can be observed that the results between the two methods are in reasonable agreement. This is interesting because for the stringer loading analysis it was assumed that the entire axle load is carried by three stringers. These results suggest that this assumption is correct for a six inch reinforced concrete deck.

Changes in the deck stiffness were investigated by increasing the deck thickness in the global FEA model. Figure 4.9 shows the loads on the 2nd from middle stringer vs. the deck thickness of both the north and southbound structures.
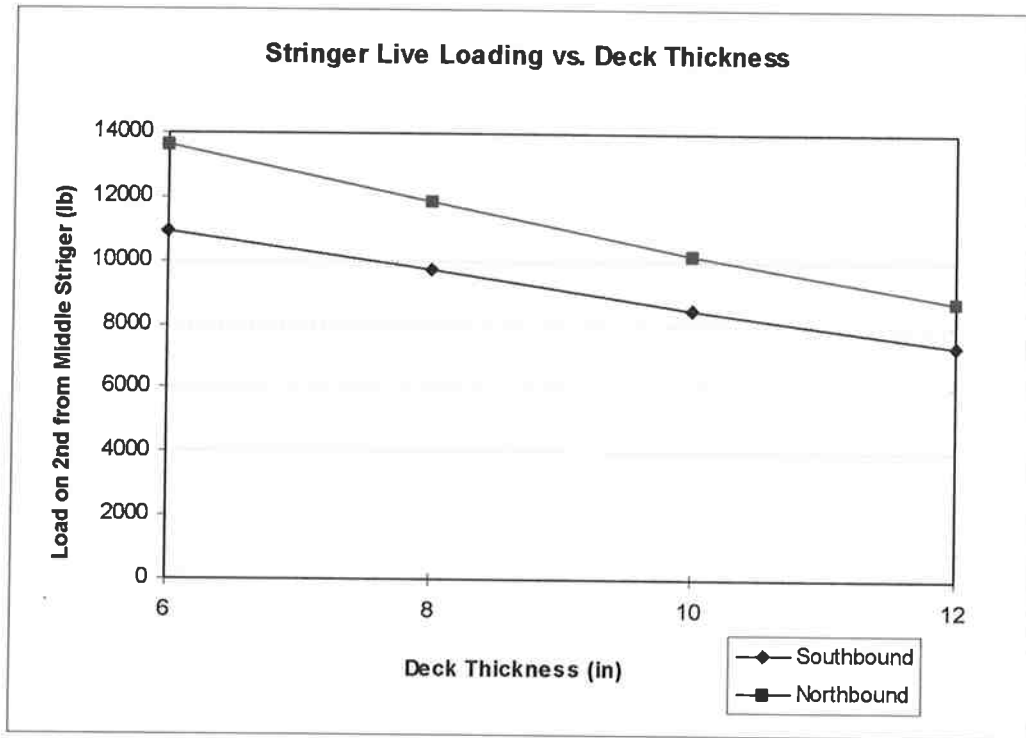
Figure 4.9 Graph of the load on the 2nd from middle stringer vs. the deck thickness from the global FEA model.

It can be observed that as the deck thickness is increased, the axle load is distributed to other stringers. This is an important discovery since the reinforced concrete deck thickness is different on other structures. Information about the effect that the deck thickness has on the loading on the stringers can easily be used to estimate the stringer loads in other bridge structures. The assumption that the effective moduli of elasticity of other bridge decks are the same as the moduli of that calculated for the Winchester Bridge would have to be accounted for in any subsequent deck stiffness analysis.

5.0 DEFLECTION AND STRESS ANALYSIS

The clip angle creates a unique boundary condition for the stringer. The compliance of this connection is somewhere between that of an ideal fixed and an ideal pinned connection. When the stringer is loaded, there is a resulting end reaction moment, M_o between the clip angle and stringer. The clip angle deflection, δ_m, the end stringer rotation, θ_{ST}, and the level of stress in the clip angle are dependent upon M_o. Since only live loading was considered, the maximum level of stress in the clip angle translates to a stress range. The three analysis techniques used to investigate these relationships are discussed in the following sections.

5.1 CLIP ANGLE DEFLECTION AND STRESS ANALYSIS

To determine the end moment, M_o, the stringer was modeled as a pinned beam with the moments, M_o, acting on the ends and the stringer load, P, acting in the middle. Figure 5.1 shows the model of the stringer.
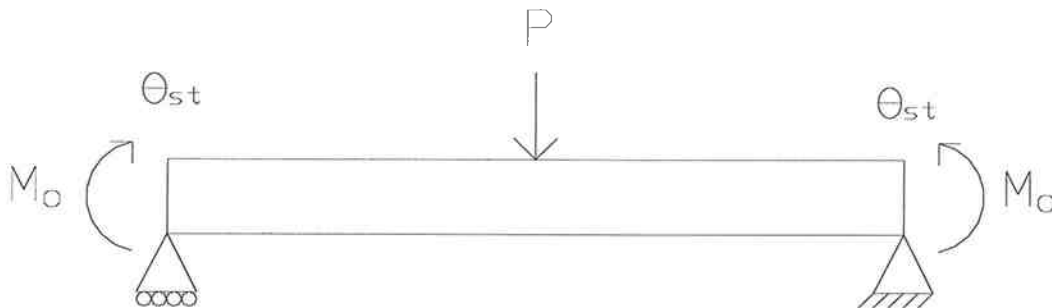
Figure 5.1 Stringer model, illustrating loading and boundary conditions.

Using beam tables from [Gere and Timshenko, 1990], the end rotation of the stringer, θ_{ST}, is written as

$$\theta_{ST} = \frac{P \cdot L^2}{16 \cdot E \cdot I} - \frac{M_o \cdot L}{2 \cdot E \cdot I} \qquad (5\text{-}1)$$

where L is the length of the stringer, I is the area moment of inertia of the stringer, and E is the Young's modulus of the stringer.

An Euler beam analysis was performed to determine the deflection of the clip angle, δ_m, as a function of the end moment, M_o. To find this relationship, the top of the floor beam leg of the clip angle was modeled as a cantilever beam with a force per unit length, F_R and a moment per unit length, M_R acting on the end. Figure 5.2 shows a diagram of the cantilever beam model of the clip angle.
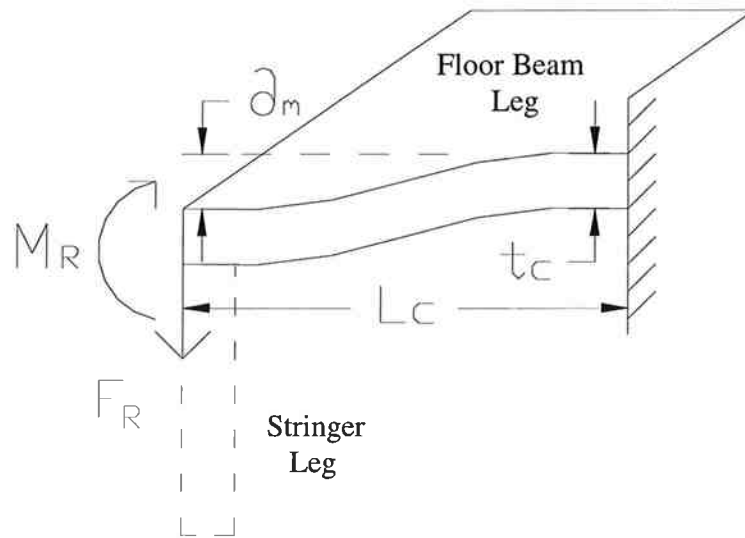
Figure 5.2 Top of the floor beam leg of the clip angle modeled as a cantilever beam.

F_R is a result of the moment, M_o, and is calculated by assuming that center of rotation of the clip angle is at the bottom. Figure 5.3 is a diagram showing how F_R is related to M_o.
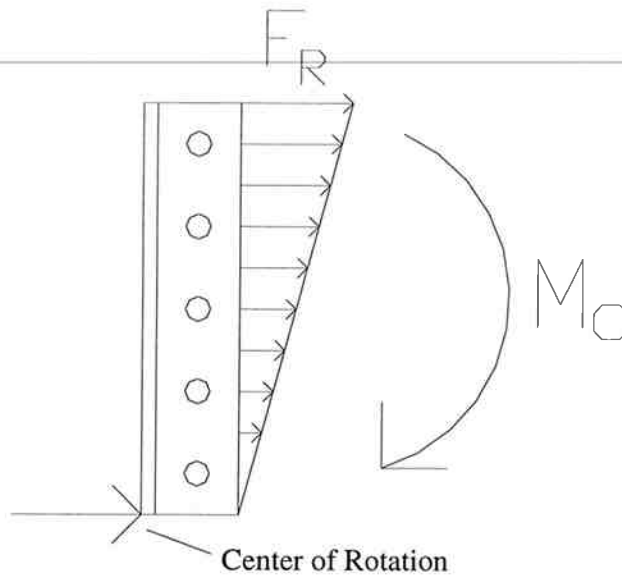
Figure 5.3 Diagram of clip angle showing the center of rotation and the relationship of F_R and M_o.

F_R is written as a function of M_o as

$$F_R = \frac{3 \cdot M_o}{2 \cdot h^2} \qquad (5\text{-}2)$$

where h is the height of the clip angle.

The stringer leg of clip angle restricts the rotation at the corner of the clip angle. For this reason, the assumption was made that rotation at the end of the beam model of the clip angle is zero. M_R is the moment at the corner of the clip angle restricting the rotation of the corner of the clip angle. By setting the end rotation equal to zero, M_R was found as a function of F_R,

$$M_R = \frac{F_R \cdot L_C}{2} \qquad (5\text{-}3)$$

where L_C is the length of the clip angle beam model. The deflection, δ_m of the clip angle was then found as a function of the end moment, M_o. The clip angle rotation is calculated (by small

angle theorem) as the deflection divided by the height of the clip angle. The expression for the clip angle rotation is

$$\theta_{cl} = \frac{\delta_m}{h} = C_R \cdot M_o \qquad (5\text{-}4)$$

$$C_R = \frac{3 \cdot L_c^3}{2 \cdot E \cdot t_c^3 \cdot h^3} \qquad (5\text{-}5)$$

where C_R is the clip angle rotation constant, L_c length of the beam, E is the Young's modulus, t_C is the clip angle thickness, and h is the height of the clip angle.

Due to physical constraints, the rotation of the clip angle and the end rotation of the stringer must be equal. The moment was found as a function of both stringer and clip angle parameters and is shown as

$$M_o = \frac{\dfrac{P \cdot L^2}{16 \cdot E \cdot I}}{C_R + \dfrac{L}{2 \cdot E \cdot I}} \qquad (5\text{-}6)$$

where P is the load on the stringer, L is the length of the stringer, I is the area moment of inertia of the stringer, E is the Young's modulus of the stringer, and C_R is the clip angle rotation constant. This equation is important because values of C_R that are determined from the results of the 3D FEA model can also be inserted into the equation above to calculate M_o. See Appendix D for details of the derivation.

The moment in the leg of the clip angle is highest at the corner of the clip angle where the stringer leg and floor beam leg of the clip angle come together. However, the maximum stress range is not located at the corner because at the corner the clip angle thickness is increased due to the corner fillet. See Appendix E for details of the calculation of the maximum stress in the clip angle. The clip angle deflections and stress ranges can be found in the results section.

5.2 2D FEA MODEL

A 2D FEA model of the top section of the clip angle was developed to determine the deflections and stress ranges in the clip angles. Plain stress plate elements of unit depth were used to build the model. Figure 5.4 shows the boundary conditions and loading of the 2D FEA model.
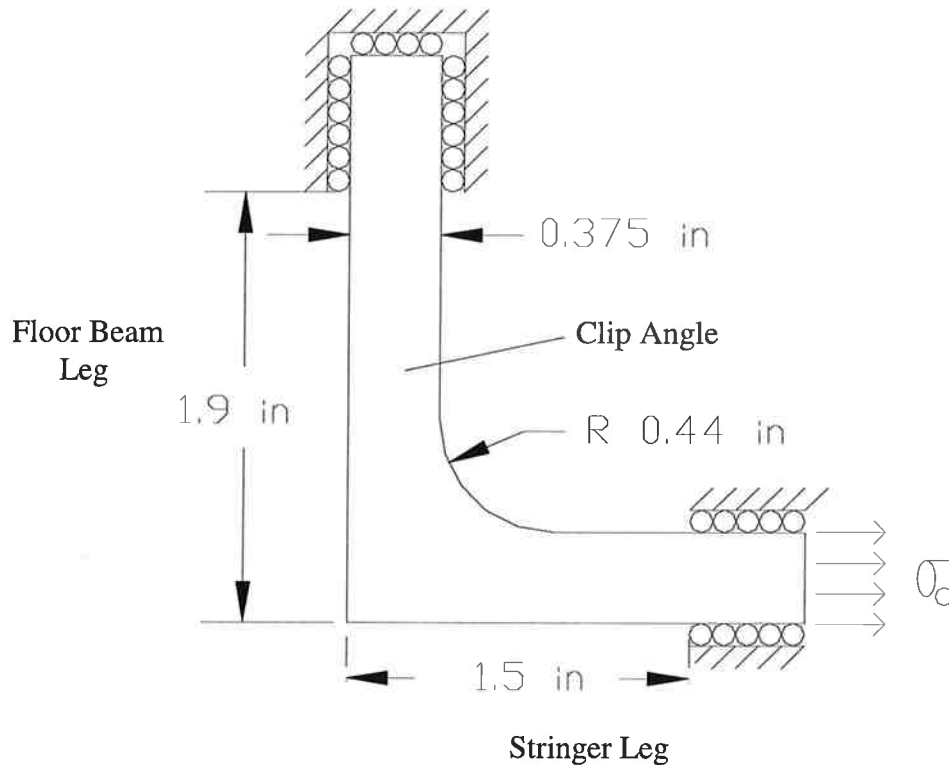
Figure 5.4 2D FEA model of the top of the clip angle illustrating size dimensions, boundary conditions, and loading.

Fixed boundary conditions were used to model the riveted connections of the clip angle to the floor beam and the stringer. The assumption was made that the riveted connections between the clip angle and the floor beam and stringer were located at the top of the clip angle, when they were actually located 1.5 inches down from the top. This simplification results in a reduction of compliance but was necessary because of the nature of the 2D model. A uniform pressure load, σ_o, was applied to the stringer leg of the clip angle to model the axial loading at the top of the clip angle from the stringer. This pressure is a result of the moment, M_o, at the end of the stringer and is found by dividing the expression for the force per unit length, F_R, by the clip angle thickness. The expression for σ_o is

$$\sigma_o = \frac{F_R}{t_C} = \frac{3 \cdot M_o}{2 \cdot t_C \cdot h^2} \tag{5-7}$$

where t_C is the thickness of the clip angle, h is the height of the clip angle, and M_o is the moment transferred to the clip angle from the stringer.

Stress ranges and deflections for the different clip angles can be found in the section 5.4. The MAZE command files and further details of the analysis can be found in Appendix F.

5.3 3D FEA MODEL

A 3D FEA model of a clip angle, a stringer, and a section of floor beam was developed to accurately determine the deflection and the stress in the clip angle. The clip angle, stringer, and floor beam were meshed as separate parts with hexahedral brick elements.

Symmetry planes were used to decrease the number of elements in the model. The model was divided into four quadrants by placing planes of symmetry both longitudinally down the center of the stringer and laterally at the mid point of the stringer.

Slide-surfaces were used as interfaces between the three parts. The contact algorithms allow non-linearity, such as gaps and frictional sliding to be modeled.

The riveted connections between the stringer, clip angle, and floor beam were important parts of the model. The rivets used to connect the stringer and clip angle were meshed as part of the stringer. The rivets used to connect the floor beam and the clip angle were meshed as part of the floor beam. Slide surfaces were used between the rivets and the clip angle. A pre-load of 25 kip was applied to the rivets to approximate the as installed rivet pre-load.

The majority of steel deck truss span bridges under the responsibility of ODOT contain connection details that are made of 3½ x 4 x ⅜ inch angles as in the Winchester Bridge and 3½ x 4 x ½ inch angles. For this reason both ⅜ inch and ½ inch thick clip angles were modeled and analyzed.

Several factors were investigated to determine their effect on the deflection and stress range of the clip angle. They are discussed in the following sections.

5.3.1 ELEMENT DENSITY

Element density was the first factor investigated. Generally, the accuracy of a finite element model increases as the number of elements increases until the mesh is sufficiently fine and

further mesh refinement does not yield a significant increase in accuracy. The analysis time is also increased as the number of elements is increased. It follows that it is desirable to use the minimum number of elements that still produce accurate results.

The effect that the element density had on the model was explored by changing the number of elements across the thickness of the clip angle. It was discovered that the deflections of the clip angle and the end rotation of the stringer did not depend significantly on the element density. The stress range did, however, depend on the density.

When the number of elements across the thickness of the $\frac{3}{8}$ inch thick clip angle was increased from four to five, the maximum stress range increased by 8%. When the number of elements was increased from five to six, the maximum stress range only increased by 4%. It was deemed that, for the $\frac{3}{8}$ inch thick clip angle, six element across the thickness was adequate.

When the number of elements across the thickness of the $\frac{1}{2}$ inch thick clip angle was increased from five to six, the maximum stress range increased by 17%. When the number of elements was increased from six to seven, the maximum stress range only increased by 5%. It was deemed that, for the $\frac{1}{2}$ inch thick clip angle, seven elements across the thickness was adequate.

5.3.2 BOUNDARY CONDITIONS

The boundary conditions for the floor beam mesh made a significant difference in the deflection and stress of the clip angle. Floor beams at the end of the span with stringers connected to only one side have different boundary conditions than floor beams in the interior of the span with stringers connected to both sides. Two sets of boundary conditions were investigated for the floor beam mesh. They were the fixed rotation model and the fixed top flange model.

The interior floor beams were modeled using the fixed rotation model. In this model, the floor beams rotation is fixed throughout the length of the mesh. The assumption was made that rotation of the interior floor beams is zero because their rotation is restricted by stringers attached to both sides.

The floor beams at the end of the span were model using the fixed top flange model. In this model, the ends of the floor beam and the top flange of the floor beam were fixed. The top flange of the floor beam was fixed to model the restriction that the reinforced concrete deck applies to the floor beam.

5.3.3 RIVET PRE-LOAD AND FRICTION

Rivet pre-load and friction were used to increase the accuracy of the riveted connection. The rivet pre-load is applied by lowering the temperature of the rivets, causing them to thermally contract. This is done in a time step before the stringer is loaded. Friction was applied by changing the coefficient of friction from 0.0 to 0.5. The static and sliding coefficients of friction for mild steel on mild steel is 0.74 and 0.57 respectively [Marks, 1996].

When the friction and rivet pre-load are applied to the model, the connection between the stringer and clip angle was changed. The rivet pre-load produces high normal forces at the interfaces between the stringer, clip angle, floor beam, and rivets. The frictional forces increase the stiffness of the connection between the stringer and the clip angle reducing the end rotation of the stringer and increasing the flexural moment transmitted to the clip angle.

The pre-load and friction also change the stress flow through the clip angle. When there is no pre-load and friction, the load from the rivet is forced to go around the rivet holes. When pre-load and friction are applied, the load is transmitted across the rivet hole by the frictional forces between the rivet, clip angle, and stringer. This results in a more localized stress concentration in the clip angle. The location of the stress concentrations will be discussed in section 5.4.

5.3.4 CLIP ANGLE THICKNESS

The clip angle thickness was another factor that was investigated. Models were created for $\frac{3}{8}$ and $\frac{1}{2}$ inch thick clip angles. For the same loading and floor beam boundary condition of fixed rotation, the deflection of the $\frac{1}{2}$ inch clip angle was 28% lower than the $\frac{3}{8}$ inch clip angle, and the maximum stress range decreased by 8%. The rotation of the end of the stringer with the $\frac{1}{2}$ inch clip angle decreased by about 12%.

The stress ranges for the different clip angles are presented in the section 5.4. The stress ranges are from models that included friction and pre-load. A TrueGrid command file and additional results can be found in Appendix G.

5.4 RESULTS

Figures 5.5 and 5.6 are exaggerated deflection plots for interior panel clip angles from the 2D FEA model and 3D FEA model, respectively.

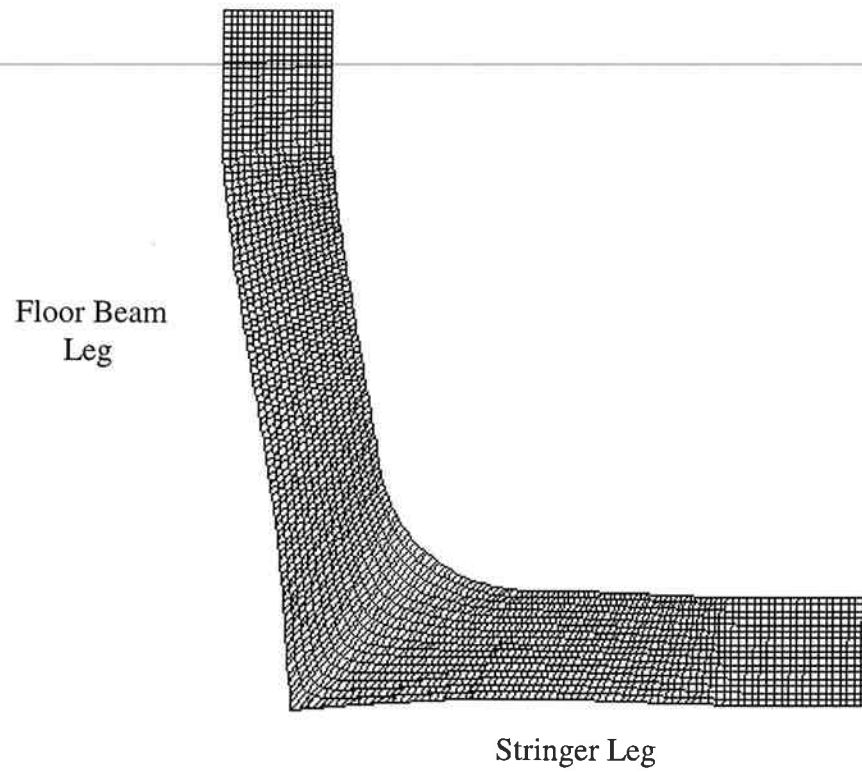Floor Beam
Leg

Stringer Leg

Figure 5.5 Exaggerated deflection plot from the 2D FEA model of an interior panel clip angle.
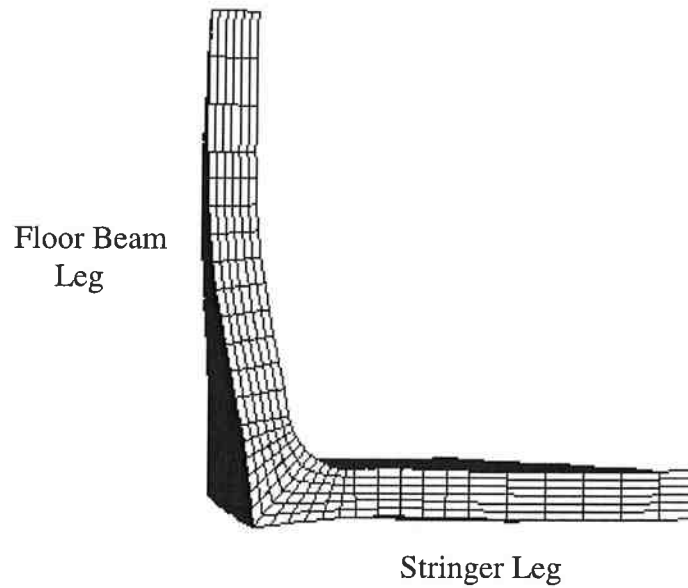
Floor Beam
Leg

Stringer Leg

Figure 5.6 Exaggerated deflection plot from the 3D FEA model of an interior panel clip angle.

The shape of the two plots appear very similar; they both show that there is rotation at the corner. This indicates that the assumption made in the clip angle deflection analysis, that the corner of the clip angle is zero, is incorrect.

The results from the clip angle deflection analysis and the 2D FEA model represent clip angles located in the interior panels only. Table 5.1 shows the deflections calculated from each analysis method for the interior panel clip angles.

Table 5.1: Comparison of Interior Panel Clip Angle Deflections (in.) from Each Analysis Method.

Analysis Method	Northbound		Southbound		
	Middle	2nd	Middle	2nd	3rd
Clip Angle Deflection Analysis	0.0019	0.0037	0.0014	0.0029	0.0021
2D FEA Model	0.0039	0.0078	0.0031	0.0061	0.0044
3D FEA Model	0.0033	0.0066	0.0025	0.0050	0.0036

The clip angle deflection analysis predicts the lowest clip angle deflection. The reason that the clip angle deflections were so low, compared to the other two analyses was the assumption of zero rotation at the clip angle corner was incorrect. Both the 2D FEA and 3D FEA deflection plots show that the rotation was restricted but not zero.

The deflection predicted from the 3D FEA model was about 16% smaller than the deflection predicted from the 2D FEA model. The reason for this is that in the 3D FEA model there was relative movement between the stringer and clip angle. In the 2D FEA model, the simplifying assumption was made that the rotation of the clip angle and rotation of the end of the stringer is the same. The relative movement adds to the compliance of the connection, reducing the flexural moment applied to the clip angle.

Figure 5.7 is a fringe plot of the maximum principle stress from the 2D FEA model. This plot is based on a 10 kip stringer load and the fringe plot displays a range of stress values from 14,000 psi to 34000 psi.

1.400E+04
1.800E+04
2.200E+04
2.600E+04
3.000E+04
3.400E+04

Floor Beam
Leg

Stringer Leg
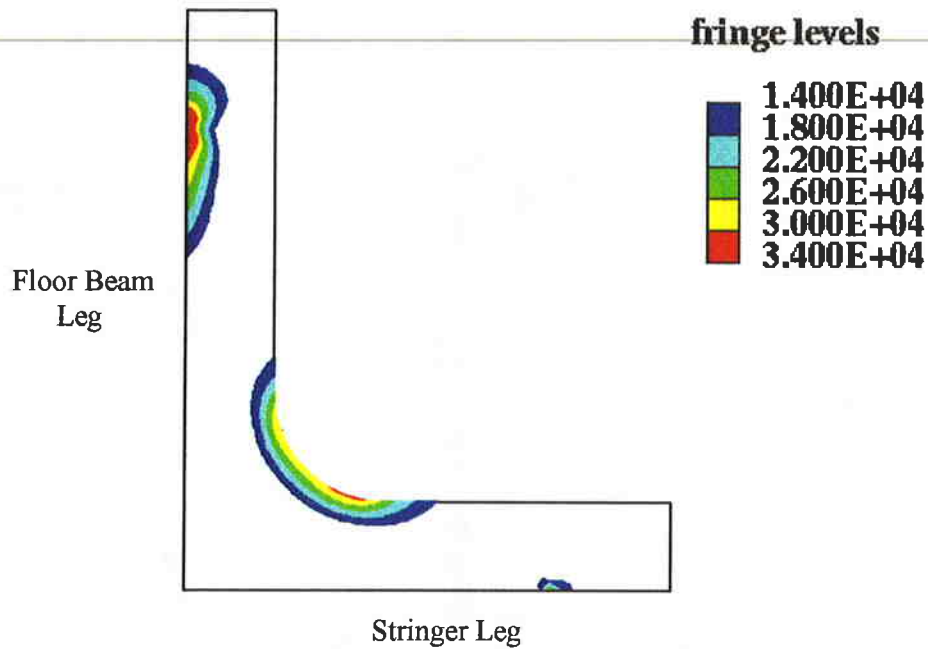
Figure 5.7 Fringe plot of the maximum principal stress for a interior panel clip
angle from the 2D FEA model.

There are two areas that achieve peak stress levels. The first is located at the base of the clip
angle where it is attached to the floor beam. This peak stress is not relevant because the riveted
connections are simplified at that location. The other peak stress area is located at the root of the
fillet on the stringer leg.

The fixed rotation model of the floor beam is used to model the clip angles attached to interior
floor beams. The fixed top flange model of the floor beam is used to model the clip angles
attached to floor beams at the end of the span. Figure 5.8 is a fringe plot of the maximum
principle stress for clip angles in the interior panels (fixed rotation model). Figure 5.9 fringe plot
of the maximum principle stress for clip angles at the end of the span (fixed top flange model). In
both cases, the stringer is loaded with 10 kip and the fringe plots display a range of stress values
from 9000 psi to 17,000 psi.

fringe levels

9.000E+03
1.060E+04
1.220E+04
1.380E+04
1.540E+04
1.700E+04

Floor Beam
Leg

Stringer
Leg

Figure 5.8 Fringe plot of the maximum principal stress from the 3D FEA
model using the fixed rotation model of the floor beam.

fringe levels

9.000E+03
1.060E+04
1.220E+04
1.380E+04
1.540E+04
1.700E+04

Floor Beam
Leg

Stringer
Leg

Figure 5.9 Fringe plot of the maximum principal stress from the 3D FEA
model using the fixed top flange model of the floor beam.

The location of the maximum stress from both 3D FEA models match the location of the maximum stress found in the 2D FEA model. The maximum stress is located at the root of the fillet on the stringer side of the clip angle. There is a l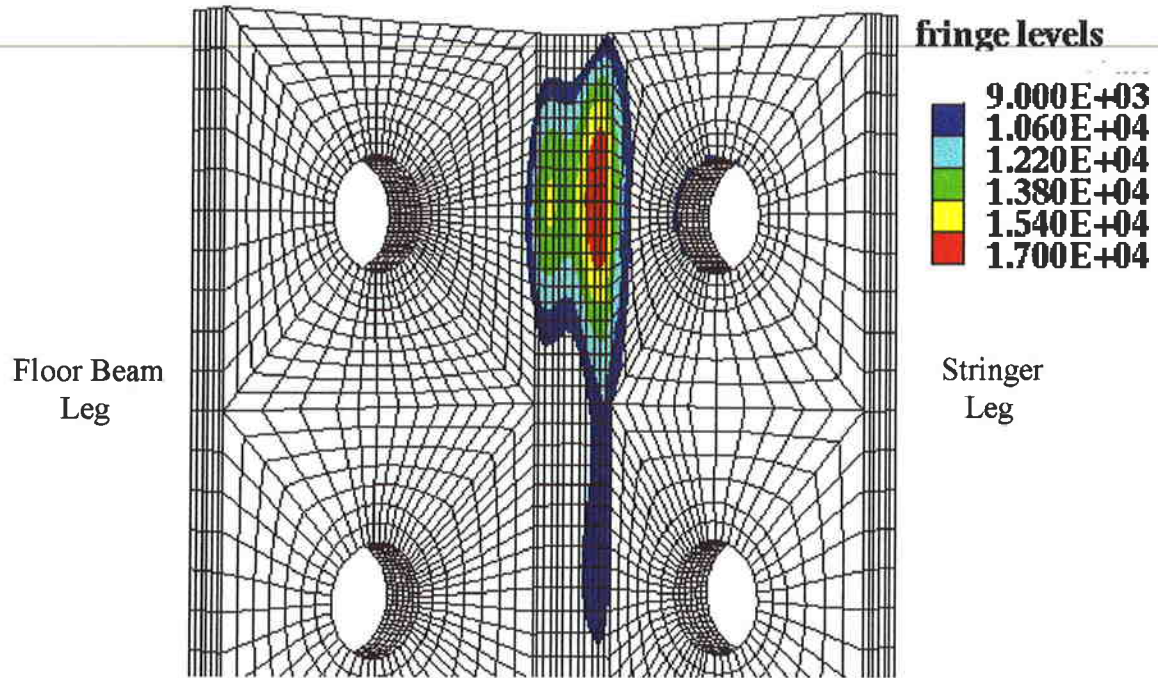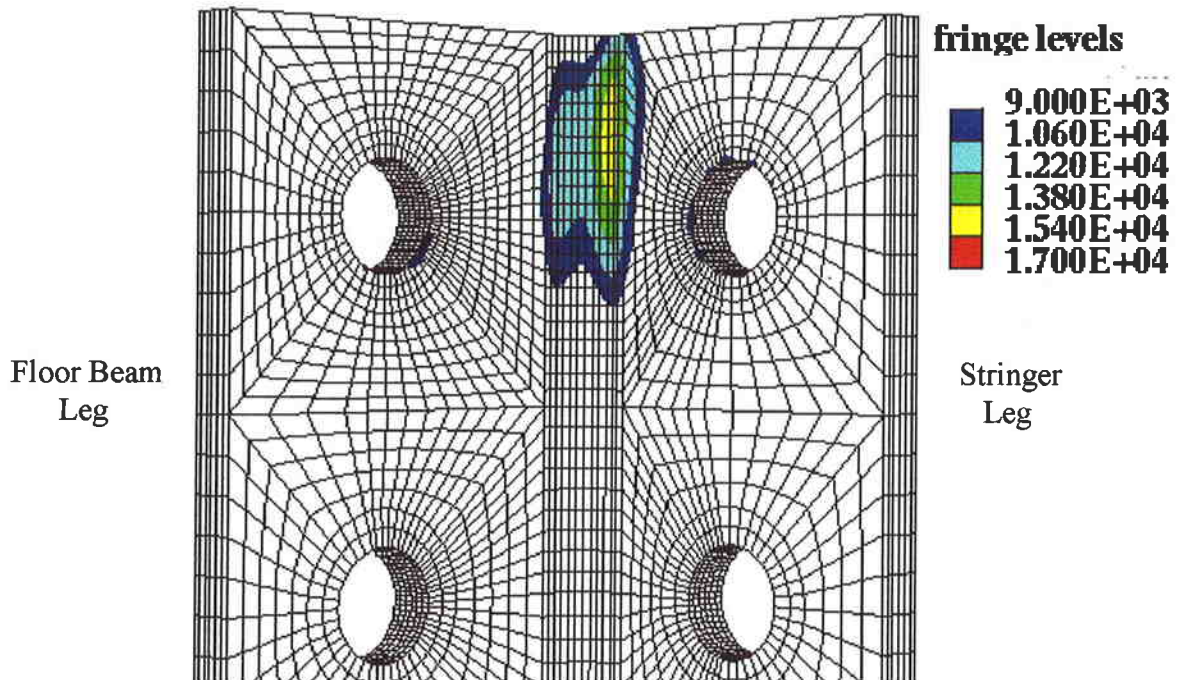ocal area of high stress at the root of the fillet on the floor beam side. This is the same location of local area of high stress calculated in the clip angle stress analysis. The stress at the root of the fillet on the floor beam side is composed only of bending stresses, while the stress at the root of the fillet on the stringer side is a combination of both axial and bending stresses.

The fixed rotation model has the highest maximum stress range. The fixed top flange model has a maximum stress range in the clip angle that is about 86% of the maximum in the fixed rotation model. The rotation of the end of the stringer in the fixed top flange model is about 46% higher than in the fixed rotation model. This is interesting because one would expect that the stress range would go down more than nine percent for such a large increase in stringer end rotation.

Table 5.2 shows the stress ranges calculated from each analysis method for interior panel clip angles.

Table 5.2: Comparison of Interior Panel Clip Angle Maximum Stress Range (ksi) Results from each Analysis Method.

Analysis Method	Northbound		Southbound		
	Middle	2nd	Middle	2nd	3rd
Clip Angle Stress Analysis	21.6	42.9	16.6	33.1	24.0
2D FEA Model	22.8	45.2	17.8	35.5	25.7
3D FEA Model	12.5	24.8	10.1	20.1	14.6

The stress ranges calculated from the 3D FEA model were much smaller than those calculated from the 2D FEA model and the clip angle stress analysis. The relative movement between the stringer and the clip angle adds to the compliance of the connection, reducing the flexural moment applied to the clip angle. This results in a reduction in the stress range.

The longitudinal positions of the clip angles affect what moment loads are transmitted to the clip angles. When a stringer is loaded, the reaction moments at each end are dependent upon the boundary conditions at both ends. Clip angles attached to floor beams at the end of the span

37

create a different boundary condition than clip angles attached to interior floor beams. Even though they represent the same boundary condition, clip angles in end panels attached to interior floor beams see higher loads than clip angles in interior panels because the other end of the stringers have clip angles that create a more compliant boundary condition. Table 5.3 shows the maximum stress ranges from the 3D FEA model for the three different longitudinal positions of the clip angles.

Table 5.3: Clip angle stress range results from the 3D FEA model for both the north and southbound structure

| Clip angle location | Northbound | | Southbound | | |
	Middle	2nd	Middle	2nd	3rd
Interior panel clip angles	12.5	24.8	10.1	20.1	14.6
End panel, interior floor beam clip angles	13.8	27.5	11.3	22.5	16.3
End panel, end floor beamclip angles	8.6	19.9	7.1	14.2	10.3

6.0 FATIGUE ANALYSIS

The stress ranges determined from the 3D FEA model using the stringer loads from the global FEA model were used in the fatigue analysis to estimate the fatigue life in load cycles of the different connection details. Two methods were used to calculate the life of the connection details. They were the stress-life approach and linear-elastic fracture mechanics approach. The strain-life approach was not used because the connection details are undergoing high cycle fatigue and the strain-life approach is only appropriate for low cycle fatigue. An overview of these three analysis methods is located in section 3.3.

Part of the analysis was to convert the fatigue life in load cycles to remaining fatigue life in years. The following sections describe the two fatigue analysis methods and the calculation of remaining fatigue life. Results of the fatigue analysis are presented in section 6.4.

6.1 STRESS-LIFE

The stress-life method is based on comparing an alternating stress amplitude to a stress vs. life curve, a S-N diagram. The constant amplitude endurance limit needs to be calculated to construct the S-N diagram. The ideal endurance limit was taken as $0.5 \cdot S_{UT}$. The ultimate tensile strength was chosen as 58 ksi, the lowest expected ultimate tensile strength for low carbon ASTM A-36 steel [Marks, 1996]. The endurance limit was then calculated by applying the following modifying factors obtained from [Shigley and Mischke, 1989].

Surface Finish - (hot rolled) $\qquad C_{SF} = 14.4 \cdot S_{UT}^{-0.718} = 0.78 \qquad$ (6-1)

Size - (thickness at fillet t = 0.5) $\qquad C_S = \left(\dfrac{t}{0.3}\right)^{-0.1133} = 0.94 \qquad$ (6-2)

Loading - (bending and axial) $\qquad C_L = 0.96 \qquad$ (6-3)

Temperature - (normal) $\qquad C_T = 1 \qquad$ (6-4)

Endurance Limit - $\qquad S_e = C_{SF} \cdot C_S \cdot C_L \cdot C_T \cdot 0.504 \cdot S_{UT} = 20.7 \text{ ksi} \qquad$ (6-5)

With the endurance limit established the S-N diagram was constructed. The equation for the number of cycles to failure is

$$N = 10^{-\frac{C}{b}} \cdot S^{\frac{1}{b}}$$

(6-6)

where $b = \frac{1}{3} \cdot \log\left(\frac{0.9 \cdot S_{UT}}{S_e}\right)$, $C = \log\left[\frac{(0.9 \cdot S_{UT})^2}{S_e}\right]$, N is the number of cycles, and S is the alternating stress amplitude.

Because of the wide range of truck sizes and weights, loading on bridges is variable in amplitude. The stress range results from the 3D FEA model are the effective variable amplitude stress ranges because the loading on the model is based on the suggested standard fatigue truck. The effective stress range obtained from the 3D FEA model was converted to an equivalent stress amplitude, S_N, using the Goodman relationship. The constant amplitude S-N relationship was then used for a variable amplitude loading by eliminating the infinite life region. The fatigue life in load cycles was then converted to remaining life in years. The remaining life of each of the different clip angles can be found in the results section. See Appendix H for details of the calculations.

6.2 LINEAR-ELASTIC FRACTURE MECHANICS

First step in determining the fatigue crack growth rate is to calculate the alternating stress intensity factor. Equation (6.2-1) from [Fisher, et al, 1989] was used to calculate the alternating stress intensity factor,

$$\Delta K = F_e \cdot F_s \cdot F_w \cdot \Delta\sigma \cdot \sqrt{\pi \cdot a}$$

(6-7)

where a is half the crack length, $\Delta\sigma$ is the alternating nominal stress, F_e is a factor for crack shape, F_s is a factor to account for a surface cracks, and F_w is a factor for a specimen with finite width.

An elliptical crack shape was assumed where a is half the length of the crack, and c is half the width of the crack. The factor F_e from [Barsom and Rolfe, 1987] is written as

$$F_e = \sqrt{\frac{1}{\phi(a)^2 + 0.5 \dfrac{\Delta\sigma}{\sigma_{ys}}}} \qquad (6\text{-}8)$$

$$\phi(a) = \int_0^{\pi/2} \left(1 - \left(\frac{c^2 - a^2}{c^2}\right)\sin(\theta)^2\right)^{\frac{1}{2}} \cdot d\theta \qquad (6\text{-}9)$$

A surface crack was assumed since the maximum stress occurs at the surface. F_s equals 1.12 for surface cracks. For surface cracks, the length a is the measurement from the surface to the crack tip. It is often referred to as the crack length instead of one half crack length.

Since the thickness of the clip angle is small, a factor from [Barsom and Rolfe, 1987] for finite width is necessary and is written as

$$F_W = 1.0 + 1.2\left(\frac{a}{t} - 0.5\right) \qquad (6\text{-}10)$$

where t is the thickness at the location of peak stress, and a is the crack length.

The next step was to solve the Paris equation for the number of cycle to failure. In order to solve the Paris equation, initial and final crack sizes were needed. The final crack size was set as the thickness of the clip angle at the point of maximum stress. Using this final crack size will result in a prediction of the number of cycles for the crack to propagate throughout the thickness of the clip angle. At this point the clip angle should be replaced.

The initial crack size is both more critical and more difficult to determine. The sizes of flaws in the clip angles vary randomly. Therefore, obtaining an accurate initial crack size is extremely difficult. The clip angles were formed by hot rolling. The surface finish for hot rolling is on the order of 0.001 inches. With a surface finish of 0.001 inches it is expected that pits and gouges on the order of 0.01 inches deep would be common. For this reason, the initial crack size of 0.01 inches was used in the model. A maximum possible flaw size was not used because the areas of maximum stress range are fairly localized. Many times, when the fracture mechanics approach is used, the initial crack size must be determined without hard data to support it.

The fatigue life, in load cycles, was then converted to remaining life in years. The remaining life of the different clip angles can be found in section 6.4. See Appendix I for details of the calculations.

6.3 REMAINING FATIGUE LIFE

This section discusses how the remaining fatigue life in years for the clip angles was calculated from the fatigue life in load cycles. The first step in calculating the remaining fatigue life was to ascertain the traffic over the Winchester Bridge. The 1994 average daily traffic (ADT) and the traffic growth rate from 1984 and 1994 for the Winchester Bridge was obtained from the 1994 Traffic Volume Tables [Oregon Department of Transportation, 1995]. The ADT was found as the linear function

$$ADT(Y) = G + g \cdot Y \tag{6-11}$$

where G is the predicted ADT for 1997, g is the growth rate, and Y is the years starting at 1997.

The percent truck traffic of the traffic was found in the 1994 Traffic Volume Tables. Average daily truck traffic (ADTT) for the slow lane of each north and southbound structure was found as

$$ADTT(Y) = \frac{ADT(Y)}{2} \cdot F_T \cdot F_L \tag{6-12}$$

where F_T is the percent truck traffic found in the 1994 Traffic Volume Tables, F_L is the percent trucks in slow lane obtained from the NCHRP Report *299* [Moses, et al, 1987]. The ADT was divided by two to find the average daily traffic for each individual structure.

The following relationship was found by taking the integral over the life of the structure,

$$N_L = D \cdot C_L \int_{-A}^{L} ADTT(Y) \cdot dY \tag{6-13}$$

where N_L is the number of load cycles to failure, D is the number of days in a year, C_L is the load cycles per truck, L is the remaining life of the detail, and A is the current age of the structure. The remaining life was found by integrating and solving for L.

6.4 RESULTS

Table 6.1 shows the remaining life in years of the different clip angles calculated using the stress-life approach. Table 6.2 shows the estimated remaining life in years of the different clip angles

calculated using the LEFM approach. When the remaining fatigue life is a negative number, it means that the fatigue analysis predicts that the clip angles should have already failed.

Table 6.1: Estimated remaining life (years) of the different clip angles calculated using the stress-life fatigue analysis.

	Northbound		Southbound		
Clip angle location	Middle	2nd	Middle	2nd	3rd
Interior panel clip angles	182	- 40	522	- 20	68
End panel, interior floor beam clip angles	100	- 42	308	- 28	22
End panel, end floor beamclip angles	1056	- 24	2340	83	477

Table 6.2: Estimated remaining life (years) of the different clip angles calculated using linear-elastic fracture mechanics

	Northbound		Southbound		
Clip angle location	Middle	2nd	Middle	2nd	3rd
Interior panel clip angles	9	- 31	35	- 18	1
End panel, interior floor beam clip angles	0	- 34	22	- 22	- 8
End panel, end floor beamclip angles	57	- 23	96	1	33

The remaining life values calculated for many of the clip angles are very low. Both models predict that both structures should have experienced extensive fatigue damage many years ago which indicates that the predicted stress ranges are probably too high. There are two explanations for why the stress ranges are high. The first is that the model of the reinforced concrete deck may not have been stiff enough. If the deck were stiffer, the loads would be distributed more evenly to other stringers. The second explanation is that an effective area

moment of inertia may need to be calculated to compensate for the composite interaction between the deck and the stringers. From equation 5.6 it can be seen that when the area moment of inertia of the stringers increase, the flexural moments seen by the clip angles decrease.

The remaining life of the clip angles at the end of the span is predicted to be much higher than for interior clip angles. This is interesting because for the southbound structure, fatigue cracks were only found in clip angles at the end of the spans. One possible explanation is that the added compliance of the connection details at the end of the span increases the tendency for them to vibrate, increasing the number of effective load cycles per truck. This would have the effect of reducing the fatigue life of those connection details. The effect of vibration on the fatigue life of the connection details was beyond the scope of the project and was not investigated.

7.0 IDENTIFICATION METHODOLOGY

There are many bridge structures under the responsibility of ODOT that are very similar to the Winchester structures. A method of quickly identifying whether or not the structure contains problem details was developed. The effects of several parameters on the stress range in the clip angles were investigated. The parameters include the reinforced concrete deck thickness, stringer spacing, stringer length, stringer area moment of inertia, and the thickness of the clip angle. Equations were developed that calculate the stress range of the clip angles that experience the highest load. A high resulting stress range would indicate that the bridge contains problem details. A decision could then be made to determine whether or not further analysis is necessary to determine which and how many details are a problem.

The effect of the reinforced concrete deck thickness on the stringer loading was investigated using the global FEA models of both the north and southbound structures. When the deck thickness is six inches, the entire axle load is distributed among three stringers. As the deck thickness is increased, the axle load is distributed to other stringers and the floor beams. The reduction of load on the stringer with the maximum load is approximately linear and is about the same for both the southbound structure (63 inch spacing) and the northbound structure (84 inch spacing). Figure 4.3-3 in section 4.3 shows the loads on the 2nd from middle stringer vs. the deck thickness of both the north and southbound structures. The effect of the deck thickness was accounted for by multiplying the maximum stringer load by a linear expression dependent only on the deck thickness.

The effect of the stringer spacing on the load of the stringers was investigated using the results from the stringer loading analysis. The stringer loading analysis was used because it does not include the effects of the deck thickness and the stringer spacing was easy to change. The load on the stringers depend on the lateral position of the axle load of the fatigue truck. Since lateral position may be unknown and the maximum stringer loads are desired, the worst case lateral position was found for each stringer spacing investigated. Figure 7.1 shows the load on the 2nd from middle stringer vs. the stringer spacing.
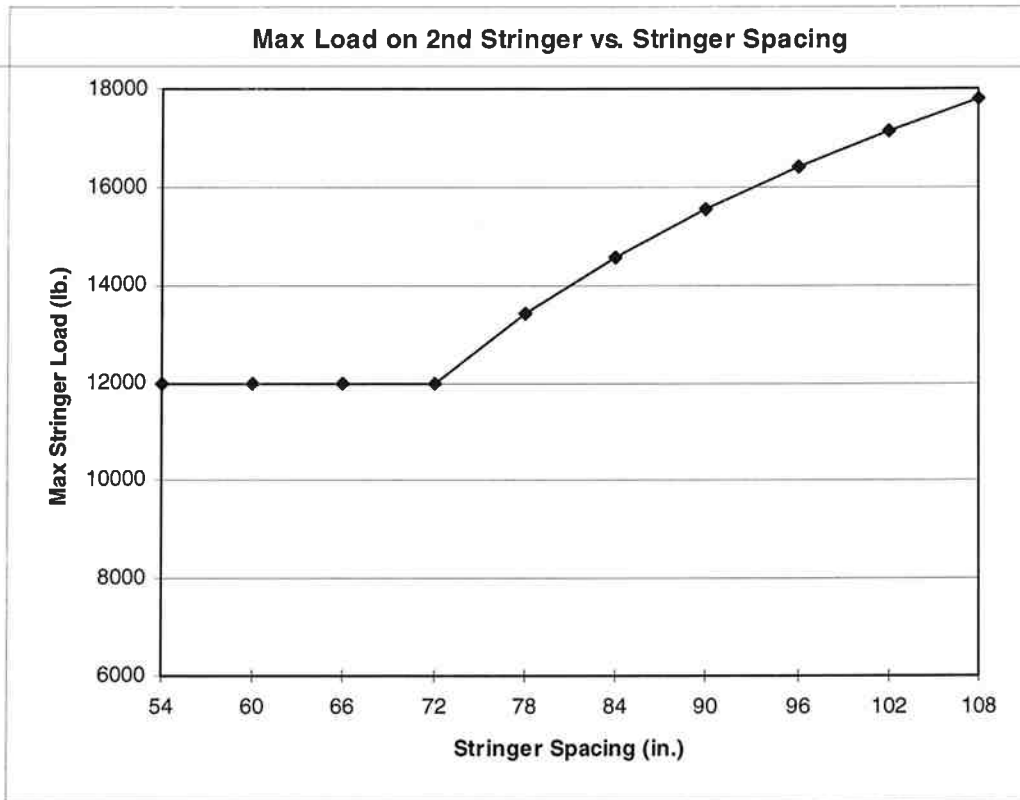
Figure 7.1 Load on the 2nd from middle stringer vs. the stringer spacing.

For a stringer spacing greater than the fatigue truck axle width (72 inches), the relationship between the maximum load and the stringer spacing is approximately linear. This maximum load occurs when the fatigue truck axle is centered over a stringer. For stringer spacing less than the fatigue truck axle width, the maximum stringer load was constant and occurred to one wheel of the axle positioned directly over the stringer. The maximum stringer load is determined by using an expression that has asymptotes of the lines in each regime. The expression for the maximum stringer load including the effects of both the reinforced concrete deck thickness and the stringer spacing is shown as

$$P = \left[12000 + \frac{S \cdot 172 - 12000}{\dfrac{72^{150}}{S^{150}} + 1} \right] \cdot \left(1 - \frac{t - 5.9}{17} \right) \tag{7-1}$$

where P is the maximum stringer load, S is the width between the stringers, and t is the thickness of the deck.

46

Equation 5-6 developed in the clip angle deflection analysis was used to calculate the end moment applied to the clip angle, based on the load on the stringer load, stringer length, stringer area moment of inertia, and the thickness of the clip angle. It is shown as

$$M_0 = \frac{\frac{P \cdot L^2}{16 \cdot E \cdot I}}{C_R + \frac{L}{2 \cdot E \cdot I}}$$
(7-2)

where M_o is the end moment applied to the clip angle, P is the maximum stringer load, L is the length of the stringer, I is the area moment of inertia of the stringer, E is Young's modulus of steel, and C_R is the clip angle rotation constant (dependent on the thickness of the clip angle).

The stress range is calculated by multiplying end moment, M_o by the clip angle stress constant C_S (dependent on the thickness of the clip angle).

$$\sigma = C_S \cdot M_O$$
(7-3)

The clip angle constants for both rotation and stress, relate the end rotation and stress in the clip angle to the end moment and are dependent on the size and shape of the clip angle. Constants are based on the results from 3D FEA model and are available for both 4 x 3½ x ⅜ and 4 x 3½ x ½ inch clip angles.

This identification methodology was developed for interior panel connection details. The recommended method of investigating a bridge is to first use the stringer area moment of inertia to calculate a stress range. If the stress range is high, a more detailed investigation should be performed using the effective area moment of inertia of the deck and stringers. The effective area moment of inertia can be determined by using strain data taken from the top and bottom flanges of several stringers loaded with a known weight. The ratio of strain between the top and bottom flanges of the stringers can be used to calculate the change in the position of the neutral axis. The known load and the strain range of the bottom flange of the stringers can be used to calculate the effective section modulus. The actual position of the neutral axis and the effective section modulus can be used to calculate the effective area moment of inertia of the stringer and deck. Using the effective area moment of inertia will give more accurate estimates for the stress range. Details of the procedure can be found in Appendix J.

8.0   RETROFIT STRATEGIES

The majority of steel deck truss span bridges under the responsibility of ODOT contain connection details that are made of $3\frac{1}{2}$ x 4 x $\frac{3}{8}$ inch clip angles (such as on the Winchester Bridge) or $3\frac{1}{2}$ x 4 x $\frac{1}{2}$ inch clip angles. Figure 2-3 in Chapter 2 illustrates the $3\frac{1}{2}$ x 4 x $\frac{3}{8}$ inch clip angle. The analysis of both of these clip angles is discussed in Chapter 5.

Five retrofit strategies were investigated to determine their effectiveness in reducing the stress range developed in the connection details. They include following:

1)   Replacing clip angles with 4 x 6 x $\frac{3}{8}$ inch angles

2)   Replacing clip angles with 4 x 6 x $\frac{1}{2}$ inch angles

3)   Removing the top row of rivets from the clip angles

4)   Removing the top two rows of rivets from the clip angles

5)   Geometric stiffening of the stringer

All of the retrofit strategies were modeled using the fixed rotation model of the floor beam, a 10 kip load, and a rivet pre-load of 25 kips. The maximum stress ranges of each retrofit strategy is compared to the maximum stress range from the 3 $\frac{1}{2}$ x 4 x $\frac{3}{8}$ inch clip angle modeled under the same loading and boundary conditions.

Retrofit strategies one and two are different only in the thickness of the angle. Figure 8.1 shows the angle used in strategy one. The new clip angles are attached to the stringers and floor beams with bolts instead of rivets. For the clip angle to stringer
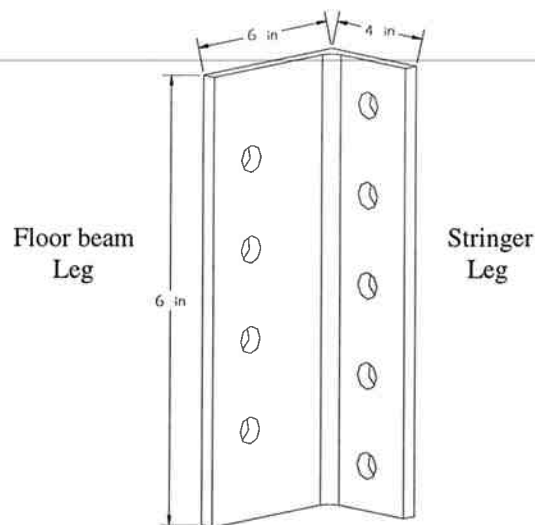
Figure 8.1 Drawing of the retrofit strategy two used to replace damaged clip angles on the Winchester Bridge in 1994.

connection, the same holes in the stringer are used for the bolts. For the clip angle to floor beam connection, the location of the holes change. Four bolts are used instead of five so that the new holes in the floor beam are located further from the old holes. This was done to retain the structural integrity of the floor beam. Strategy two was used to replace damaged clip angles on the Winchester Bridge in 1994.

Retrofit strategies one and two were designed to increase the compliance of the clip angle. The longer floor beam leg increases the compliance of the connection reducing the flexural moment transmitted to the clip angle. The resulting deflection from strategy one is 10% more than that of the $\frac{3}{8}$ inch clip angle. The resulting deflection from strategy two is 5% more than that of the $\frac{3}{8}$ inch clip angle. The stress range for strategy one is 75% of the stress range for the $\frac{3}{8}$ inch clip angle. The stress range for strategy two is 60 % of the stress range for the $\frac{3}{8}$ inch clip angle.

The results show that increasing the compliance does reduce the stress range in the clip angle. It is also apparent that increasing the thickness of the clip angle reduces the stress range in the clip angle.

Retrofit strategies three and four involve removing rivets from the existing clip angles. In strategy three, the top row of rivets that attach the clip angle to the floor beam and stringer are removed. In strategy four, the top two rows of rivets that attach the clip angle to the floor beam and stringer are removed. Strategy four also includes installing a bracket under the stringer to relieve the shear load on the remaining three rows of rivets. The bracket was located in the model so that it supported the stringer directly under the location of the stringer rivets.

Retrofit strategies three and four are also designed to increase the compliance of the connection. They are different from strategies one and two because compliance is added to the connection

between the clip angle and stringer, not in the clip angles themselves. The stress range for strategy three is 68% of the stress range for the ⅜ inch clip angle. The stress range for strategy four is 30% of the stress range for the ⅜ inch clip angle. The bracket used to transmit shear loads did not significantly affect the stress range in the clip angle.

In retrofit strategy five, geometric stiffening is achieved by attaching one inch diameter, high strength, wire rope to the bottom of the stringer. The wire rope is fastened to the bottom flange at each end of the stringer. At mid span, the wire rope is attached to a strut that pushes the rope 12 inches below the bottom of the stringer. Figure 8.2 shows a diagram of the retrofit strategy five. The wire rope is pre-loaded to a stress of 6 ksi. When the wire rope is pre-loaded, a force is applied to the stringer that opposes the live
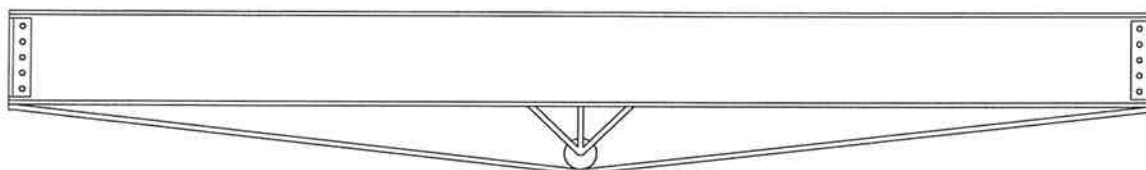

Figure 8.2 Diagram of the retrofit strategy five, geometric stiffening.

loading on the stringer. The wire and stringer also form a truss structure that increases the stiffness of the assembly. As the stringer is loaded, the wire rope resists the deflection of the stringer. The tension of the wire rope will pull on the bottom flange of the stringer resisting the end rotation. Also, as the tension increases a force at the strut will be applied upward to the stringer that will oppose the load on the stringer. The stress range for the strategy five with a one inch diameter wire rope pre-loaded at 6 ksi is 76% the stress range of the ⅜ inch clip angle.

Table 8.1 shows a summary of the retrofit strategies and their relative effectiveness.

Table 8.1: Effectiveness of the Five Retrofit Strategies Investigated.

Retrofit strategy	$\dfrac{\sigma \text{ (retrofit)}}{\sigma \text{ (⅜ in angle)}}$
1) 4 x 6 x ⅜ inch angle	0.73
2) 4 x 6 x ½ inch angle	0.60
3) Removing top row of rivets	0.68
4) Removing top two rows of rivets	0.30
5) Geometric stiffening	0.76

9.0 SUMMARY AND CONCLUSIONS

The Winchester Bridge is a typical steel deck truss bridge under the responsibility of the Oregon Department of Transportation that contains connection details that are fatigue prone. Although the primary function of the clip angles is to transmit end shear from the stringers to the floor beams, because the clip angles are riveted to both the stringers and floor beams, they are subjected to a flexural moment caused by the deflection of the stringer under live truck loads.

Even though strain data taken from the bridge, indicates that the remaining fatigue life estimates are very conservative, the analysis indicates that the connection details are very prone to fatigue damage.

A low cost field identification methodology was developed to determine whether other steel deck truss bridges contain problem details. The effects of parameters for the reinforced concrete deck thickness, stringer spacing, stringer length, effective stringer area moment of inertia, and thickness of the clip angle have been quantified. Equations were developed to quickly and easily estimate the stresses in the clip angles under the highest loads. The recommended method of investigating a bridge is to first use the stringer moment of inertia. If the stress range is high, a more detailed investigation should be performed using the effective area moment of inertia of the deck and stringers. The effective area moment of inertia would be obtained experimentally.

Five retrofit strategies were investigated to determine their effectiveness at reducing the stress range in the clip angles. The most effective method is retrofit strategy four (removing the top two rows of rivets). Retrofit strategy four is the recommended strategy because it is both very effective and easy to implement. It involves less installation work than replacing the clip angles as in strategies one and two and requires less design work than strategy five. Removing only the top row of rivets in strategy three would be easier to implement than strategy two but it is just not as effective at reducing the stress range as removing the top two rows of rivets.

REFERENCES

Bannantine, J. A., Comer, J. J., and Handrock, J. L., 1990, *Fundamentals of Metal Fatigue Analysis*, Prentice-Hall, Inc., Englewood Cliffs, NJ.

Barsom, J. M., and Rolfe, S. T., 1987, *Fracture & Fatigue Controls in Structures*, 2nd Edition, Prentice-Hall, Inc., Englewood Cliffs, NJ.

Cao, L., Allen, J. H., Shing, P. B., and Woodham, D., 1996, "Behavior of RC Bridge Decks with Flexible Girders", Journal of Structural Engineering, American Society of Civil Engineers, New York, NY.

Christon, M. A., and Dovey, D., 1992, *INGRID User's Manual*, Lawrence Livermore National Laboratory, Livermore, CA.

COSMOS/M User's Guide, 1993, Volume 1, Version 1.70, Structural Reserch and Analysis Corporation, Santa Monica, CA.

Engelmann, B., 1991, *NIKE2D User's Manual*, Lawrence Livermore National Laboratory, Livermore, CA.

Everard, N. J., and Tanner, J. L., 1966, *Reinforced Concreate and Design*, McGraw-Hill Inc. , New York, NY.

Fisher, J. W., Mertz, D. R., and Zhong, A., 1983, "Steel Bridge Members Under Variable Amplitude Long Life Fatigue Loading." *NCHRP Report 267*, p. 22, Transportation Research Board, Washington, DC.

Fisher, J. W., Yen, B. T., and Wang, D., 1989, "Fatigue of Bridge Structure - A Commentary and Guide For Design, Evaluation and Investigation of Cracking." *ATLSS Report No. 89-02*, Lehigh University, Bethlehem, PA.

Gere, J. M., and Timoshenko, S. P., 1990, *Mechanics of Materials*, 3rd Edition, PWS-KENT, Boston, MA.

Hallquist, J. O., and Levatin, J. L., 1985, *ORION User's Manual*, Lawrence Livermore National Laboratory, Livermore, CA.

Hallquist, J. O., 1983, *MAZE User's Manual*, Lawrence Livermore National Laboratory, Livermore, CA.

LS-NIKE3D User's Manual, 1996,Version 970, Livermore Software Technology Corporation, Livermore, CA.

"LS-TAURUS User's Manual: Appedix J", 1995, *LS-DYNA3D User's Manual*, Version 936, Livermore Software Technology Corporation, Livermore, CA.

Maker, B. N., 1991, *NIKE3D User's Manual*, Lawrence Livermore National Laboratory, Livermore, CA.

Marks, Lionel S., 1996, *Marks' Standard Handbook for Mechanical Engineers*, 10th ed. McGraw-Hill, Inc., New York, NY.

Moses, F., Schilling, C. G., and Raju K. S., 1987, *NCHRP Report 299 Fatigue Evaluation Procedures for Steel Bridges*, Transportation Research Board, Washington, DC.

Shigley, J. E., and Mischke, C. R., 1989, *Mechanical Engineering Design*, 5th Edition, McGraw-Hill, Inc., New York, NY.

TrueGrid Manual, 1995, Version 0.99, XYZ Scientific Applications, Inc., Livermore, CA.

Wilson, W. M., "Design of Connection Angles for Stringers of Railway Bridges", 1940, University of Illinois.

Wilson, W. M., and Coombe, J. V. 1939, "Fatigue Tests of Connection Angles", Engineering Experiment Station Bulletin Series No 317, University of Illinois.

Oregon Department of Transportation, 1995, 1994 Traffic Volume Tables, Transportation Development Branch, Oregon Department of Transportation, Salem, OR.